nature cell biology

Myofibril contraction and crosslinking drive nuclear movement to the periphery of skeletal muscle

William Roman[1,2,3], João P. Martins[3], Filomena A. Carvalho[3], Raphael Voituriez[4,5], Jasmine V. G. Abella[6], Nuno C. Santos[3], Bruno Cadot[1,2], Michael Way[6] and Edgar R. Gomes[1,2,3,7]

Nuclear movements are important for multiple cellular functions, and are driven by polarized forces generated by motor proteins and the cytoskeleton. During skeletal myofibre formation or regeneration, nuclei move from the centre to the periphery of the myofibre for proper muscle function. Centrally located nuclei are also found in different muscle disorders. Using theoretical and experimental approaches, we demonstrate that nuclear movement to the periphery of myofibres is mediated by centripetal forces around the nucleus. These forces arise from myofibril contraction and crosslinking that 'zip' around the nucleus in combination with tight regulation of nuclear stiffness by lamin A/C. In addition, an Arp2/3 complex containing Arpc5L together with γ-actin is required to organize desmin to crosslink myofibrils for nuclear movement. Our work reveals that centripetal forces exerted by myofibrils squeeze the nucleus to the periphery of myofibres.

Nuclear positioning within cells is important for multiple cellular activities during development, immune response, tissue homeostasis and regeneration[1]. Moreover, nuclear positioning defects result in multiple human disorders such as lissencephaly, deafness and muscle disorders[2,3]. The mechanisms of nuclear positioning involve cytoskeletal networks and motor proteins. In most cases, the nucleus is connected to the cytoskeleton by nuclear envelope proteins or by the nuclear pore complex[4–8]. Microtubules or actin growing towards the nucleus, as well as active diffusion can also drive nuclear movement[9–11].

The most diversified example of nuclear positioning occurs during skeletal muscle differentiation. Muscle fibres (myofibres) are multinucleated cells that are formed by the fusion of mononucleated muscle precursor cells (myoblasts)[12]. Nuclei are initially in the centre of the myofibre and then move towards the myofibre periphery during myogenesis[13].

We recently showed that nuclear positioning within myofibres is required for proper muscle function[14]. In addition, several monogenic muscle disorders and regenerating muscle exhibit centrally located nuclei[15–18]. The architecture of skeletal muscle is designed for its contractile purpose. Sarcomeres, the contractile unit, are connected to one another longitudinally by the z-line and form bundles named myofibrils that span the entire length of the myofibre[19]. These myofibril bundles are crosslinked by desmin networks connected at the z-line. Desmin is a cytoplasmic intermediate filament that is expressed in muscle cells in place of vimentin, with both of these proteins sharing similar molecular and cellular functions[20,21]. Myofibrils are surrounded by transversal triads, specialized junctions composed of t-tubules and sarcoplasmic reticulum. These structures are responsible for excitation–contraction coupling, allowing the transduction of electric membrane potentials into muscle contractions[22]. Myofibrils are formed during gestation and surround the centrally located nuclei. The positioning of nuclei at the periphery occurs near birth whereas transversal triads are formed only at a later stage in the first postnatal weeks[23].

We recently found that BIN1/amphiphysin-2 (mutated in centronuclear myopathies) interacts with N-WASP and both are required for actin-dependent peripheral nuclear movement and transversal triad formation[24]. These results imply a role for actin that is nucleated by the Arp2/3 complex[25–27], in nuclear movement to the periphery. Here we confirm this hypothesis and provide the mechanism of nuclear movement to the periphery of myofibres.

[1]Sorbonne Universités, UPMC Univ Paris 06, INSERM UMRS974, CNRS FRE3617, Center for Research in Myology, GH Pitié-Salpêtrière, 47 Boulevard de l'Hôpital, 75013 Paris, France. [2]Centre de Référence de Pathologie Neuromusculaire Paris-Est, Institut de Myologie, GHU La Pitié-Salpêtrière, Assistance Publique-Hôpitaux de Paris, 75013 Paris, France. [3]Instituto de Medicina Molecular, Faculdade de Medicina, Universidade de Lisboa, Avenida Professor Egas Moniz, 1649-028 Lisboa, Portugal. [4]Laboratoire de Physique Théorique de la Matière Condensée, CNRS UMR 7600, Université Pierre et Marie Curie, 75013 Paris, France. [5]Laboratoire Jean Perrin, CNRS FRE 3231, Université Pierre et Marie Curie, 75013 Paris, France. [6]Cellular Signalling and Cytoskeletal Function Lab, The Francis Crick Institute, 1 Midland Road, London NW1 1AT, UK.
[7]Correspondence should be addressed to E.R.G. (e-mail: edgargomes@medicina.ulisboa.pt)

Received 16 June 2016; accepted 4 August 2017; published online 11 September 2017; DOI: 10.1038/ncb3605

RESULTS

Nuclei are squeezed by myofibrils when moving to the myofibre periphery

To investigate the mechanism of nuclear movement to the periphery of muscle cells, we used an *in vitro* myofibre system that recapitulates the embryonic and neonatal development of muscle fibres[23,24,28]. After three days, myofibres with myofibrils exhibit centrally located nuclei and no transversal triads. Between days 4–6, nuclei move to the periphery followed by transversal triad organization at day 7 (Fig. 1a).

We performed three-dimensional (3D) time-lapse spinning-disc microscopy of these differentiated *in vitro* myofibres labelled for myofibrils and nuclei between day 4.5 and 5.5. Before movement to the periphery, centrally located nuclei are surrounded by myofibril bundles (Supplementary Fig. 1A and Supplementary Video 1). The movement of the nucleus to the periphery begins with the emergence of an elongated nuclear wrinkle through a narrow gap in between myofibrils (Fig. 1b,c). With time the wrinkle increases into a protrusion and the nucleus undergoes a dramatic deformation. This results in the nucleus being expelled from the middle of the myofibril bundle to the myofibre periphery in the direction of the nuclear protrusion over a period of 145 ± 41 min, with an average speed of 2.4 $\mu m\, h^{-1}$ (Supplementary Video 2). The deformation and protrusion of nuclei reaching the periphery of myofibres was also observed *in vivo* (Fig. 1d,e) and by electron microscopy (Fig. 1f,g).

Desmin crosslinks myofibrils for nuclear movement to the myofibre periphery

Quantification of 3D nuclear shape reveals that the nucleus sphericity and volume decrease prior to protrusion and emergence before being re-established as the nucleus emerges at the periphery (Fig. 2a,b and Supplementary Fig. 1B,C).

When analysing the middle plane of the myofibre, we observed an area next to the nucleus where myofibrils were not present due to deflection around the nucleus (Figs 1c and 2c), which was also observed by electron microscopy (Supplementary Fig. 1D). This area decreases prior to nuclear movement as though myofibrils crosslink and 'zip' together towards the nucleus (Fig. 2d). Next we used laser ablation to disrupt crosslinking between myofibrils labelled with YFP-α-actinin. Following ablation with high-powered laser, both nuclear sphericity and volume increased, which was not observed following bleaching with low-powered laser (Fig. 2e–g and Supplementary Fig. 1E). Both adjacent myofibril distance and myofibre thickness increased following ablation (Supplementary Fig. 1F). We fixed the cells after ablation and stained for α-actinin to confirm that high-power laser was ablating myofibrils whereas low-power laser was only bleaching the YFP signal without disrupting myofibrils (Supplementary Fig. 1E). Overall, these data suggest an increase in the forces applied to the nucleus by myofibril zipping around the nucleus before the initiation of nuclear movement to the periphery.

Desmin is an intermediate filament known to crosslink myofibrils at the z-line and was implicated in nuclear positioning in muscle[18,29–31]. Depletion of desmin by short interfering RNA (siRNA)-mediated knockdown impairs nuclear movement to the periphery (Fig. 3a,b and Supplementary Fig. 2A,B) without disruption of myofibril structure or contraction frequency (Supplementary Fig. 2C–E). Expression of human EmGFP-desmin, resistant to mouse siRNA, restored nuclear movement (Fig. 3c). Furthermore, the desmin network is already organized at the z-line before nuclear movement but only in sections of the myofibres away from centrally located nuclei. Desmin is disorganized near centrally located nuclei in the area devoid of myofibrils (Fig. 3d). When we visualized EmGFP-desmin during nuclear movement to the periphery we observed the organization of desmin in striations towards the nucleus, similar to myofibril zipping (Figs 1c and 3e). These data suggest that myofibril crosslinking and zipping by desmin leads to the squeezing of the nucleus to the cell periphery.

γ-actin is required for nuclear movement and desmin organization

We next explored how nuclear positioning to the periphery is regulated, taking into account our previous study showing that BIN1/amphiphysin-2, which is mutated in centronuclear myopathies, triggers peripheral nuclear positioning via N-WASP and actin[24]. Six actin isoforms are expressed in mammals, of which three are found in skeletal muscle: α-, β- and γ-actin. α-actin is the main sarcomeric actin, required for sarcomere formation. We therefore focused our analysis on the cytoplasmic actins namely γ- and β-actin, known to have different functions (Supplementary Fig. 3A)[32,33]. We found that siRNA-mediated depletion of γ-actin, but not β-actin, inhibits nuclear positioning (Supplementary Figs 3B–D and 4A,C). In contrast, β-actin depletion, but not γ-actin, inhibits transversal triad formation (Fig. 4a–c). We confirmed these results by performing rescue experiments with siRNA-resistant GFP-tagged γ-actin and β-actin (Supplementary Fig. 3e–g).

The actin cytoskeleton associates and organizes vimentin intermediate filaments in different cellular events such as cell migration[34,35]. As vimentin and desmin share multiple structural, biochemical and physiological properties, actin could be involved in the organization of desmin in skeletal muscle[20]. Accordingly, γ-actin-depleted, but not control or β-actin-depleted myofibres lack desmin organization at the z-line (Fig. 4d).

The Arp2/3 complex is required for nuclear movement and desmin organization

We previously showed that N-WASP, which stimulates the actin-nucleating activity of the Arp2/3 complex[25–27], is required for peripheral nuclear positioning[24]. We therefore tested the role of the Arp2/3 complex in nuclear movement[25–27] (Supplementary Fig. 4A). Depletion of Arpc2, essential for Arp2/3 nucleation activity[36,37], inhibits nuclear movement, but not myofibril formation (Supplementary Fig. 4B–E). Furthermore, transversal triad formation, which occurs later on during myofibre differentiation, is also inhibited (Supplementary Fig. 4B–E). These results were confirmed by Arp2/3 complex inhibition with CK666 (ref. 38) (Supplementary Fig. 4E).

Arp2/3 complexes differ in their actin assembly activity depending on the isoforms of Arpc1 (Arpc1A and Arpc1B) and Arpc5 (Arpc5 and Arpc5L)[39]. We found that depletion of Arpc1A or Arpc1B prevents both peripheral nuclear positioning and transversal triad formation (Supplementary Fig. 4F,G). However, depletion of Arpc5L, but not Arpc5, inhibits only nuclear positioning (Fig. 4e–g). In contrast, loss of Arpc5, but not Arpc5L, blocks transversal triad formation but not nuclear positioning (Fig. 4e–g and Supplementary Fig. 4H–J). We additionally found that Arpc5L-depleted, but not control or Arpc5-depleted myofibres lack desmin organization at the z-line (Fig. 4h).

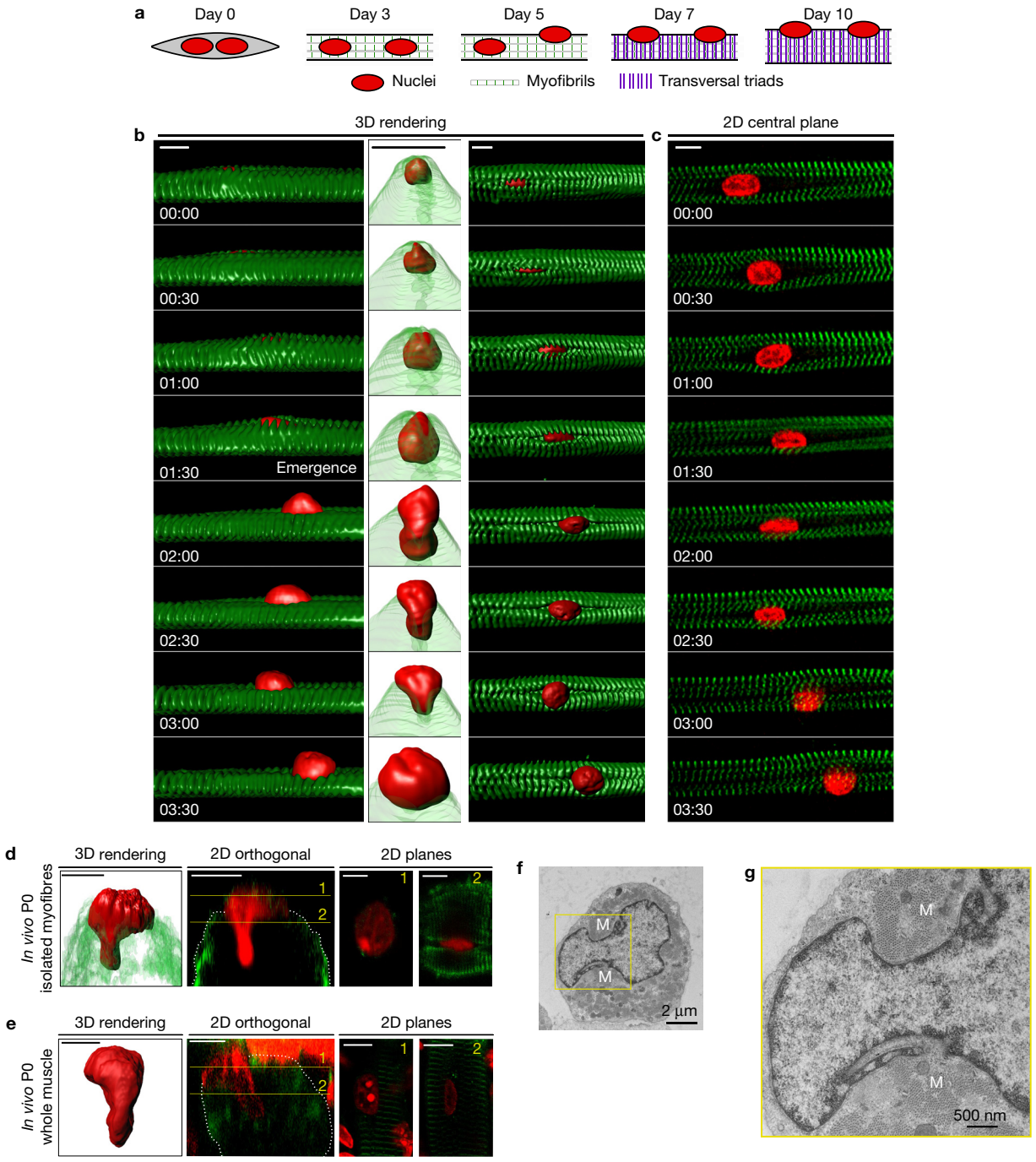

Figure 1 Visualizing nuclear movement to the periphery. (**a**) Timeline of muscle differentiation in the *in vitro* system used to study peripheral nuclear positioning and transversal triad formation. Nuclei are in red, myofibrils are in white (with z-lines in green) and transversal triads as purple lines. Day 3: myofibril formation. Day 5: initiation of peripheral nuclear positioning. Day 7: transversal triad formation. (**b**) Kymograph from a time-lapse video of a 5-day myofibre depicting peripheral movement of a nucleus (H2B-iRFP, red) through myofibrils (YFP-α-actinin, green). Left: view from the side, surface 3D rendering. Middle: view from the right side, with transparent myofibril 3D rendering. Right: view from the top, surface 3D rendering. Time, hh:mm. Scale bars, 10 µm. (**c**) 2D view of the central plane of a kymograph from a time-lapse video of a 5-day myofibre depicting peripheral movement of a nucleus (H2B-iRFP, red) through myofibrils (YFP-α-actinin, green). Scale bar, 10 µm. (**d**) Representative images of a nucleus squeezing to the periphery from an *in vivo* isolated myofibre of a newborn (P0) mouse and stained for myofibrils (α-actinin, green) and nucleus (red). Left: 3D rendering. Middle left: 2D orthogonal view; the yellow lines represent the slices seen in the right panels. Middle right: 2D plane from yellow slice 1. Right: 2D plane from yellow slice 2. Scale bars, 10 µm. The images shown are representative of two experiments. (**e**) Representative images of a nucleus squeezing to the periphery after performing a clearing protocol of a whole muscle in a newborn mouse and stained for myofibrils (α-actinin, green) and nucleus (red). Left: 3D rendering. Middle left: 2D orthogonal view; the yellow lines represent the slices seen in the right panels. Middle right: 2D plane from yellow slice 1. Right: 2D plane from yellow slice 2. Scale bars, 10 µm. The images shown are representative of two experiments. (**f**) Transversal electron micrograph of a 4.5-day myofibre showing a nucleus beginning to protrude towards the periphery. 'M' annotates myofibrils. (**g**) Magnification (×4) corresponding to the yellow square in **f**. The image shown is representative of four experiments.

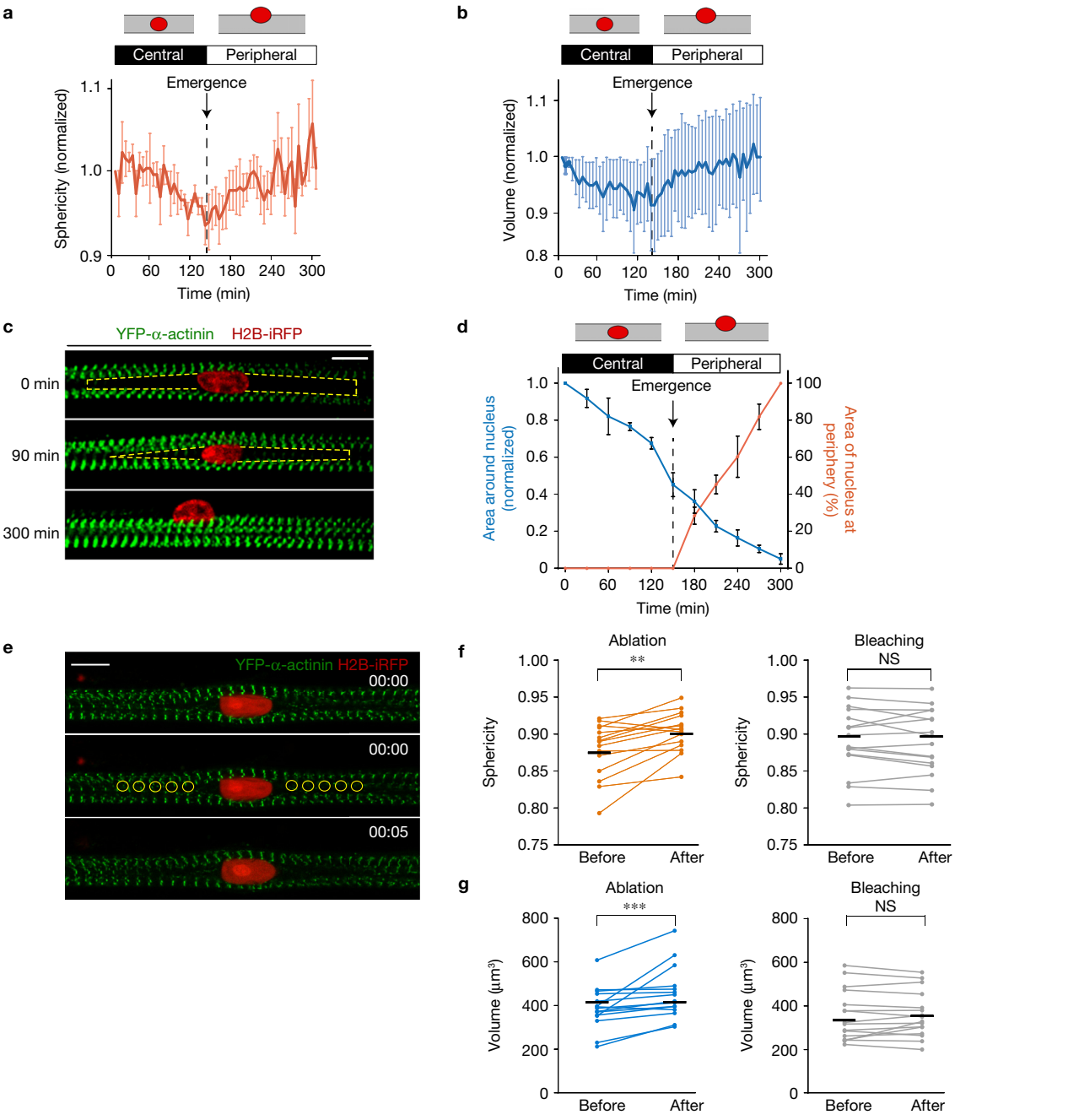

Figure 2 Myofibre crosslinking drives nuclear movement to the periphery. (**a**) Quantification of the sphericity of nuclei during nuclear movement to the periphery in 5-day myofibres. The dashed line corresponds to the emergence of the nucleus at the myofibre periphery ($n=8$ myofibres). Data from six independent experiments were combined. Error bars correspond to s.e.m. Source data are available in Supplementary Table 3. (**b**) Quantification of the volume of nuclei during nuclear movement to the periphery in 5-day myofibres. The dashed line corresponds to the emergence of the nucleus at the myofibre periphery ($n=8$ myofibres). Data from six independent experiments were combined. Error bars correspond to s.e.m. Source data are available in Supplementary Table 3. (**c**) Kymograph from a time-lapse video of a 5-day myofibre depicting the area around the nucleus in between myofibrils (yellow dashed line) during nuclear movement to the periphery with the nucleus (H2B-iRFP, red) migrating through myofibrils (YFP-α-actinin, green). Scale bar, 10 μm. (**d**) Quantification of the area in between myofibrils around the nucleus (blue line) and the percentage of area of the nucleus at the periphery over time (orange line) in 5-day myofibres ($n=8$ myofibres). Error bars correspond to s.e.m. Source data are available in Supplementary Table 3. (**e**) Representative images of a 4.5-day myofibre time-lapse video before and after laser ablation with myofibrils depicted in green (YFP-α-actinin) and the nucleus in red (H2B-iRFP). The yellow circles represent ablation areas performed at 00:00 (hh:mm). Scale bar, 10 μm. The images shown are representative of six experiments. (**f**) Dot plot showing changes in nuclei sphericity before and after ablation (orange) or bleaching (grey). The black lines represent the average. Data from three independent experiments were combined ($n=15$ nuclei). Wilcoxon matched-pairs signed ranked test was used to determine statistical significances; $^{**}P<0.01$; NS, not significant. Source data are available in Supplementary Table 3. (**g**) Dot plot showing changes in nuclei sphericity before and after ablation (blue) or bleaching (grey). The black lines represent the average. Data from three independent experiments were combined and error bars represent s.e.m. from $n=15$ nuclei. Wilcoxon matched-pairs signed ranked test was used to determine statistical significances; $^{***}P<0.001$; NS, not significant. Source data are available in Supplementary Table 3.

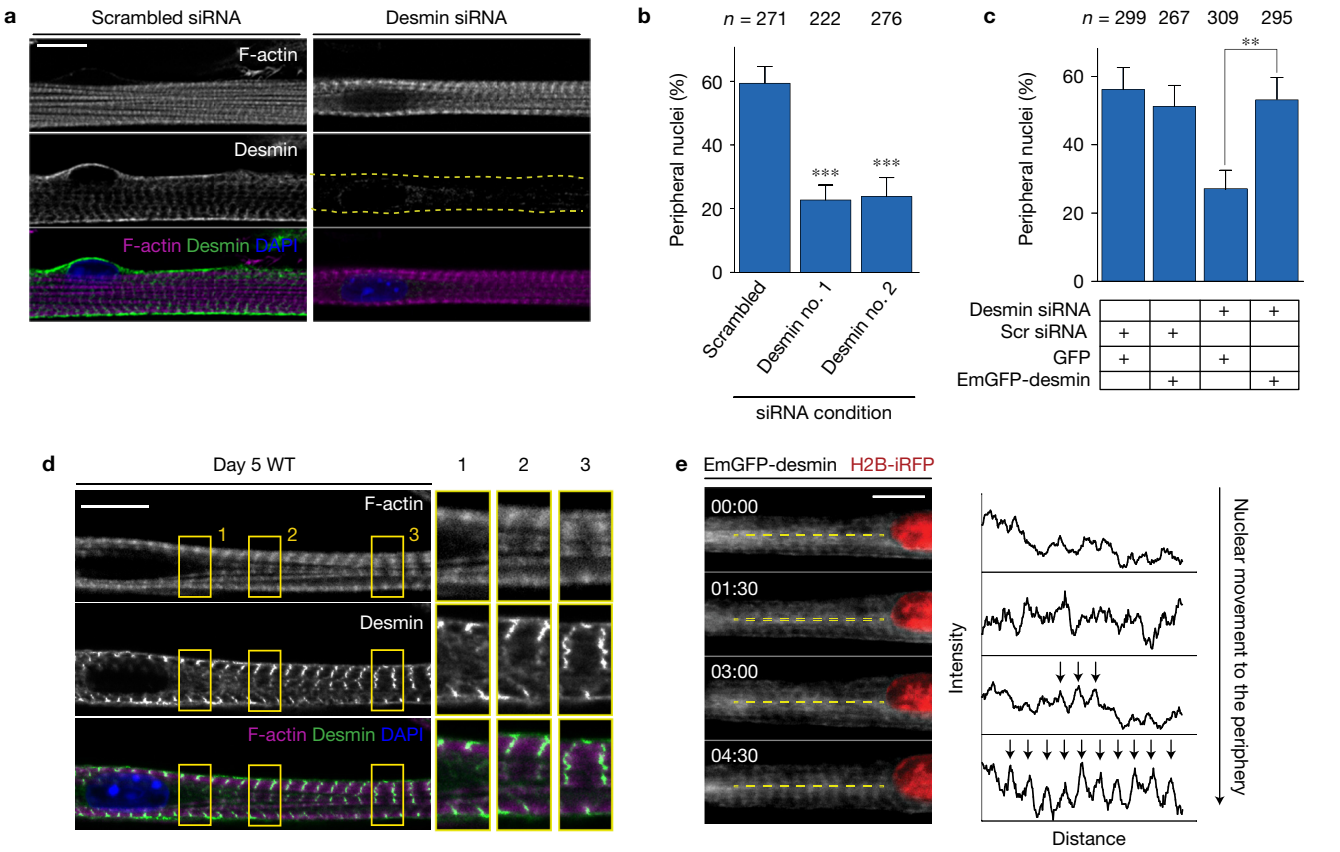

Figure 3 Desmin crosslinks myofibrils to induce nuclear movement to the periphery. (**a**) Representative immunofluorescence image of a 10-day myofibre knocked down for scrambled or desmin and stained for F-actin (phalloidin, magenta), desmin (green) and DAPI (nucleus, blue). Scale bar, 10 μm. (**b**) Quantification of peripheral nuclei positioning in 10-day myofibres knocked down for scrambled or desmin. Data from three independent experiments were combined and error bars represent s.e.m. from indicated *n* nuclei for each cohort. Unpaired *t*-test was used to determine statistical significances; $^{***}P < 0.001$. Source data are available in Supplementary Table 3. (**c**) Quantification of peripheral nuclei positioning and traversal triads in 10-day myofibres knocked down for scrambled or desmin and transfected with either GFP or EmGFP-desmin. Data from three independent experiments were combined and error bars represent s.e.m. from indicated *n* nuclei for each cohort. Unpaired *t*-test was used to determine statistical significances; $^{**}P < 0.01$. (**d**) Representative immunofluorescence images of a 4.5-day myofibre stained for F-actin (phalloidin, magenta), desmin (green) and DAPI (nucleus, blue). Magnifications (×2) corresponding to the yellow squares are shown on the right corresponding to areas near the nucleus with disorganized desmin either without (1) or with (2) myofibrils, or areas away from the nucleus with organized desmin and myofibrils (3). Scale bar, 10 μm. The images shown are representative of three experiments. (**e**) Kymograph from a time-lapse video of a 5-day myofibre depicting desmin organization, showing Emerald-desmin (EmGFP-desmin, grey) during nuclear movement to the periphery (H2B-iRFP, red). The yellow dashed lines represent the region used to perform line scans plotted on the right. The arrows highlight the transversal organization of desmin. Time, hh:mm. Scale bar, 10 μm. Source data are available in Supplementary Table 3.

Our finding that γ-actin and Arpc5L are involved in nuclear positioning prompted us to test whether these two proteins interact in myofibres. We found that γ-actin co-immunoprecipitates with GFP-tagged Arpc5L but not Arpc5 (Fig. 5a). Conversely, Arpc5L, but not Arpc5, co-immunoprecipitates with GFP-γ-actin (Fig. 5b). In all situations, Arpc2 also co-immunoprecipitates. Finally, endogenous γ-actin co-immunoprecipitates with endogenous Arpc5L, but not Arpc5 (Fig. 5c). Consistent with this, Arpc5L and γ-actin co-localize in small patches between myofibrils near centrally located nuclei in 5-day myofibres (Fig. 5d). In contrast, Arpc5 and β-actin are transversally organized (Supplementary Fig. 5A,B). The number of γ-actin patches was reduced following depletion of Arpc5L, but not Arpc5 (Supplementary Fig. 5C,D). The co-localization of Arpc5L and γ-actin occurs in areas depleted of myofibrils where desmin is not organized (Fig. 5e). We also determined that Arpc5L and γ-actin depletion does not affect desmin expression (Supplementary Fig. 5E,F); however, it impairs desmin dynamics as measured by fluorescence recovery after photobleaching of EmGFP-desmin (Supplementary Fig. 5G,H).

To further understand how the Arp2/3 complex and γ-actin organize desmin, we explored the role of plectin, a cytoskeletal linker that connects desmin to the z-line[40]. We found that plectin is required for nuclear positioning and desmin organization, but not for myofibril formation (Fig. 5f,g and Supplementary Fig. 5I–K). Plectin is at the z-line just before nuclear movement, independently of Arpc5L or γ-actin (Fig. 5h). Furthermore, plectin is already at the z-line prior to desmin and peripheral nuclear movement (Supplementary Fig. 5L). This shows that Arpc5L and γ-actin organize the desmin cytoskeleton downstream or in parallel to plectin for nuclear movement.

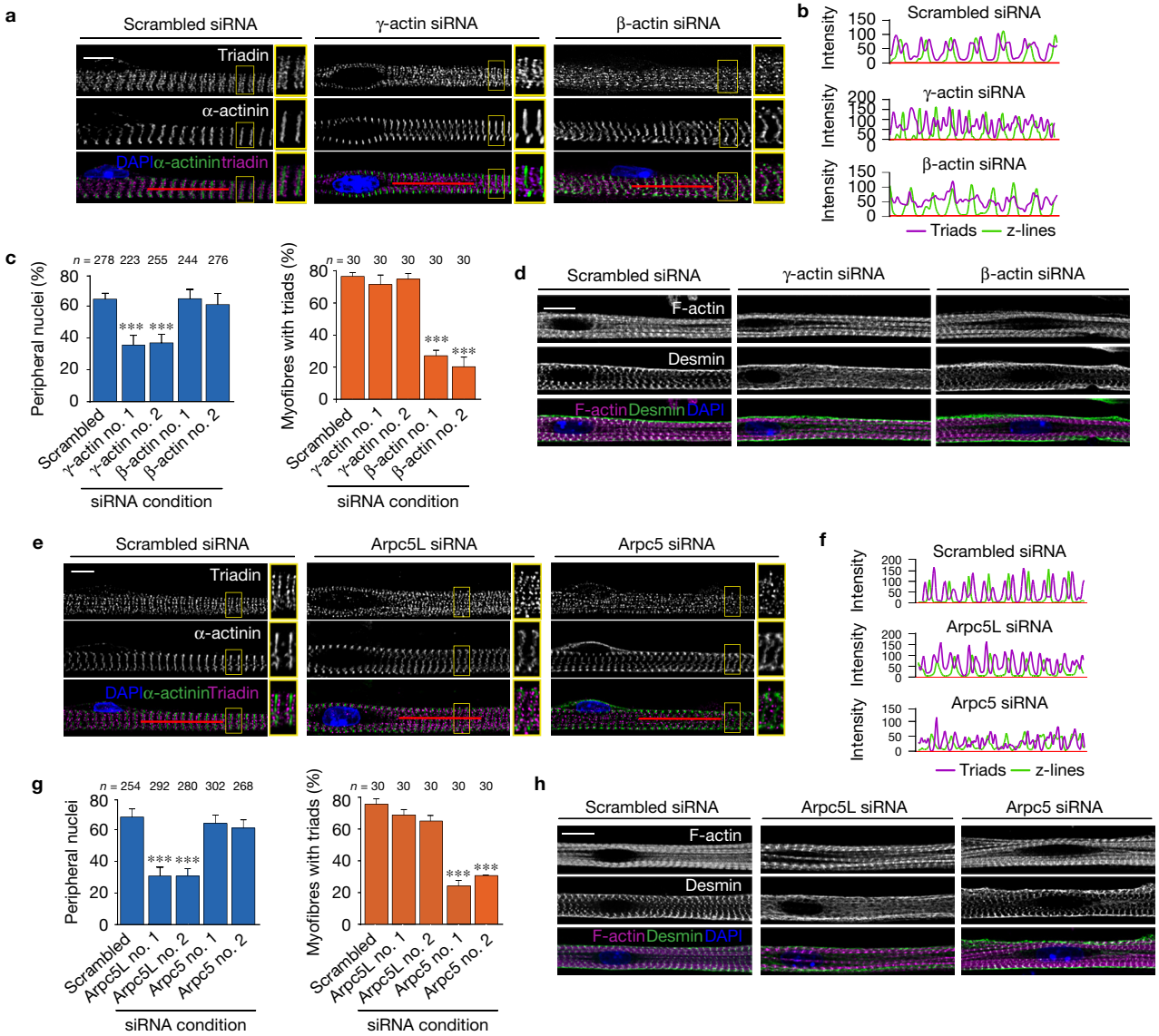

Figure 4 Actin and Arp isoforms play different roles in myofibre differentiation. (**a**) Representative immunofluorescence images of a 10-day myofibre knocked down for scrambled, γ-actin or β-actin and stained for triadin (triad marker, magenta), α-actinin (myofibrils/z-line marker, green) and DAPI (nucleus, blue). Scale bar, 10 μm. Magnifications (×2) corresponding to the yellow squares are shown on the right of each image. The images shown are representative of three experiments. (**b**) Line scans of the red line depicted in **a** to visualize the organization of transversal triad doublets (magenta) and z-line (green) in scramble, γ-actin or β-actin-knockdown myofibres. (**c**) Quantification of peripheral nuclei positioning (left) and transversal triad formation (right) in 10-day myofibres knocked down for scrambled, γ-actin or β-actin. Data from three independent experiments were combined and error bars represent s.e.m. from indicated *n* nuclei or myofibres for each cohort. Unpaired *t*-test was used to determine statistical significances; $^{***}P<0.001$. Source data are available in Supplementary Table 3. (**d**) Representative images of 5-day myofibres knocked down for scramble, γ-actin or β-actin and stained for F-actin (phalloidin, magenta), desmin (green) and DAPI (nucleus, blue). Scale bar, 10 μm. The images shown are representative of three experiments. (**e**) Representative immunofluorescence images of 10-day myofibres knocked down for scrambled, Arpc5L or Arpc5 and stained for triadin (triad marker, magenta), α-actinin (myofibrils/z-line marker, green) and DAPI (nucleus, blue). Scale bar, 10 μm. Magnifications (×2) corresponding to the yellow squares are shown on the right of each image. The images shown are representative of three experiments. (**f**) Line scan of the red line depicted in **e** to visualize the organization of transversal triad doublets (magenta) and of z-line (green) in scramble-, Arpc5l- or Arpc5-knockdown myofibres. (**g**) Quantification of peripheral nuclei positioning (left) and transversal triad formation (right) in 10-day myofibres knocked down for scrambled, Arpc5L or Arpc5. Data from three independent experiments were combined and error bars represent s.e.m. from indicated *n* nuclei or myofibres for each cohort. Unpaired *t*-test was used to determine statistical significances; $^{***}P<0.001$. Source data are available in Supplementary Table 3. (**h**) Representative images of 5-day myofibres knocked down for scramble, Arpc5L or Arpc5 and stained for F-actin (phalloidin, magenta), desmin (green) and DAPI (nucleus, blue). Scale bar, 10 μm. The images shown are representative of three experiments.

A theoretical model for nuclear movement to the myofibre periphery

We developed a theoretical model of nuclear movement to the periphery. Before peripheral movement, the nucleus (of radius $R_0 \approx 6\,\mu m$) is wrapped by a bundle of $N \approx 30$ myofibrils[41] and centred along the symmetry axis of the bundle. Each myofibril is modelled as an active spring, whose relaxed tension ($T \approx 1$ to 10 nN) is induced by myofibrils at the measured sarcomere length of 2.7 μm (Fig. 6a)[42]. Myofibril

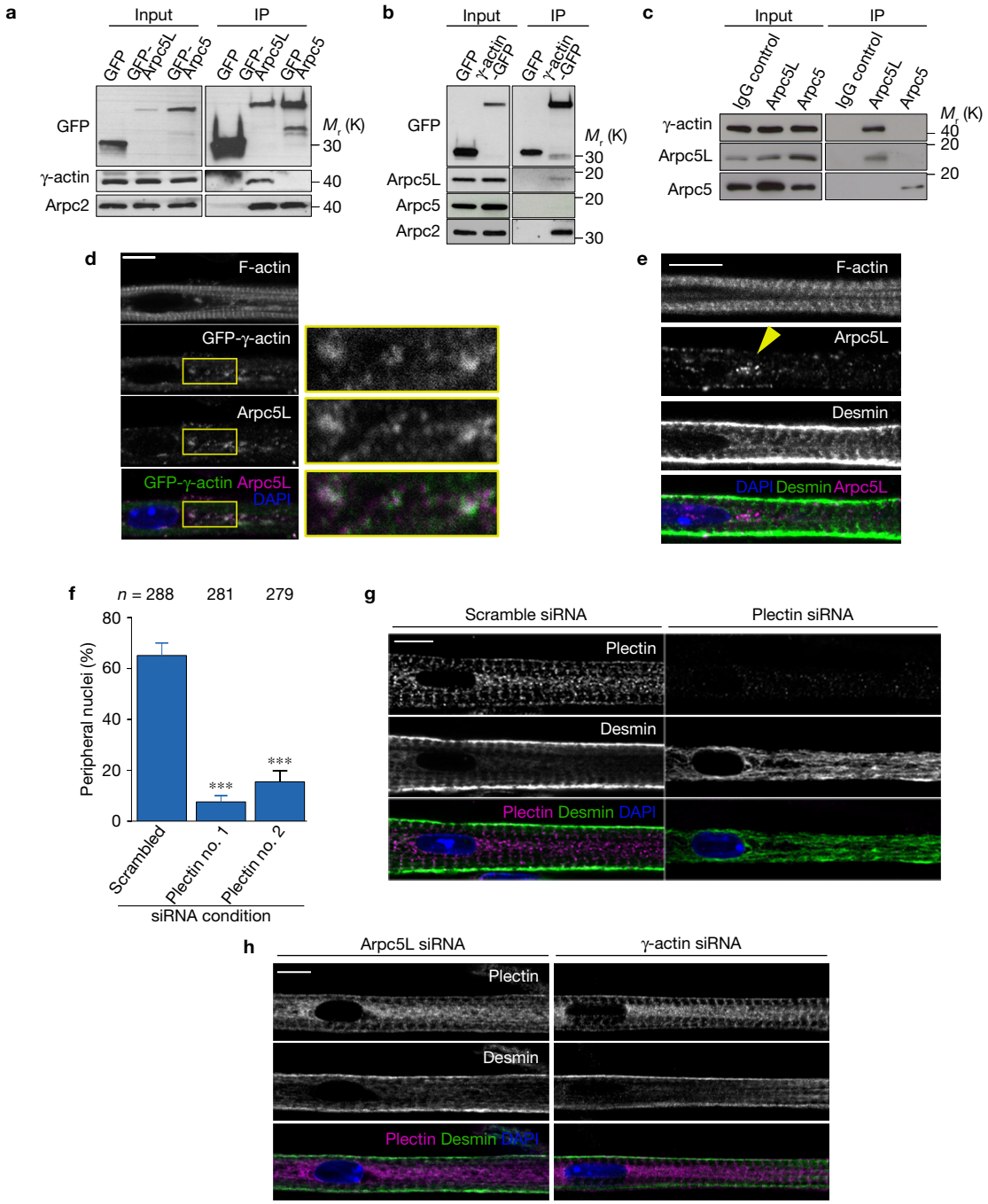

Figure 5 Arpc5L and γ-actin interact to crosslink myofibrils. (**a**) Western blots with the indicated antibodies of GFP, GFP-Arpc5L or GFP-Arpc5 immunoprecipitated from 5-day myofibres. Experiments were performed three times. (**b**) Western blots with the indicated antibodies of GFP and GFP-γ-actin immunoprecipitated from 5-day myofibres. Experiments were performed three times. (**c**) Western blots with the indicated antibodies of IgG control, Arpc5L and Arpc5 immunoprecipitated from 5-day myofibres. Experiments were performed three times. (**d**) Representative immunofluorescence images of 5-day myofibres expressing GFP-γ-actin (green) and immunostained for Arpc5L (magenta) in 5-day myofibres (left). Scale bar, 10 μm. Magnifications (×3) corresponding to the yellow rectangle are shown on the right. The images shown are representative of three experiments. (**e**) Representative immunofluorescence images of 5-day myofibres stained for Arpc5L (magenta), desmin (green) and F-actin. The yellow arrowhead points to the area depleted of myofibrils in which desmin is disorganized and Arpc5L is enriched. Scale bar, 10 μm. The images shown are representative of three experiments. (**f**) Quantification of peripheral nuclei positioning in 10-day myofibres knocked down for scrambled or plectin. Data from three independent experiments were combined and error bars represent s.e.m. from indicated *n* nuclei for each cohort. Unpaired *t*-test was used to determine statistical significances; $^{***}P < 0.001$. Source data are available in Supplementary Table 3. (**g**) Representative immunofluorescence images of a 4.5-day myofibre knocked down for scrambled or plectin and stained for plectin (magenta), desmin (green) and DAPI (nucleus, blue). Scale bar, 10 μm. The images shown are representative of three experiments. (**h**) Representative immunofluorescence images of a 4.5-day myofibre knocked down for Arpc5L or γ-actin and stained for plectin (magenta), desmin (green) and DAPI (nucleus, blue). Scale bar, 10 μm. The images shown are representative of three experiments. Unprocessed original scans of blots are shown in Supplementary Fig. 9.

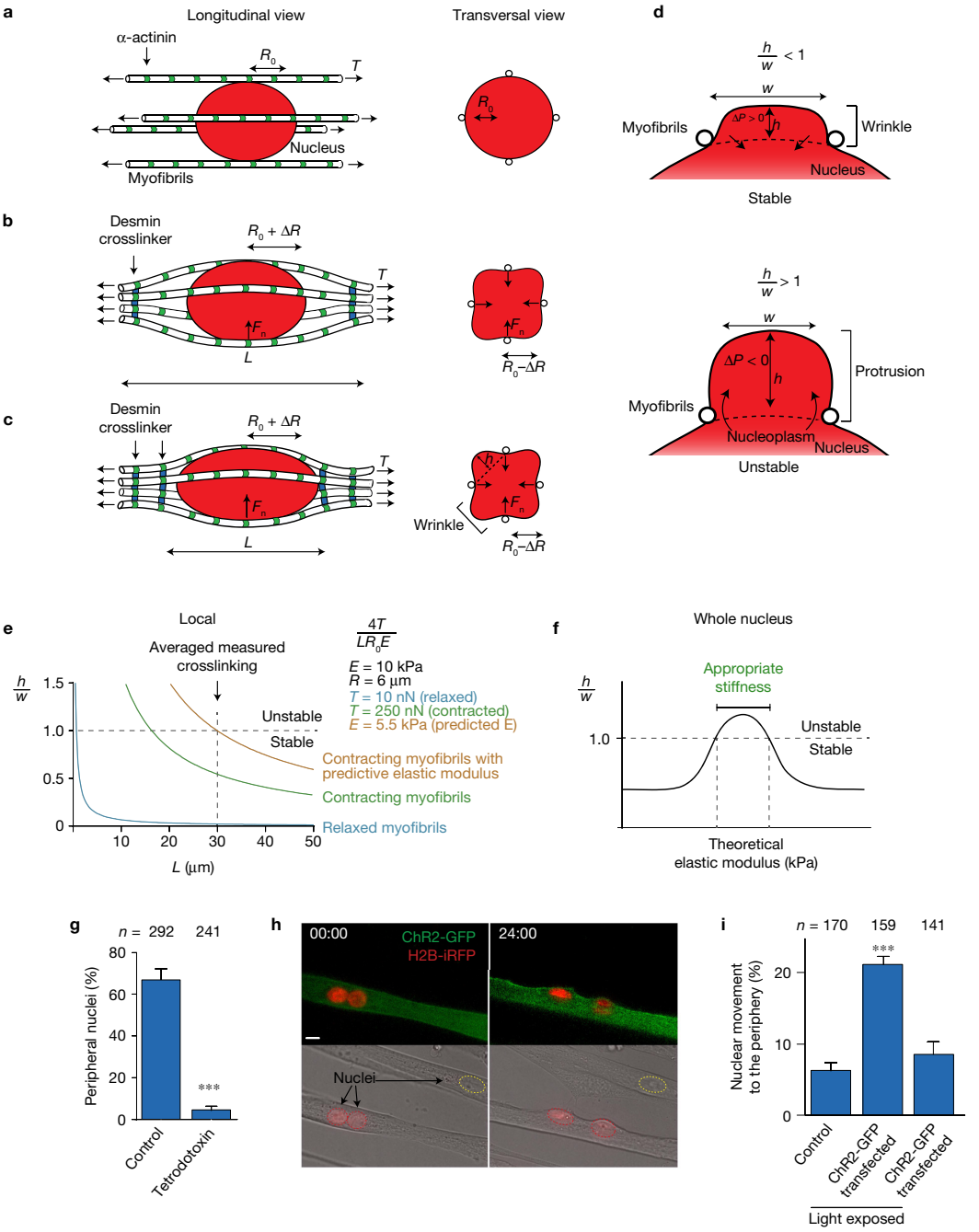

Figure 6 Theoretical model of peripheral nuclear movement and role of contraction. (**a**–**c**) Schematic of a nucleus (red) surrounded by myofibrils (white) before (**a**) and during (**b**,**c**) peripheral migration. Longitudinal view (left) and transversal view (right). R_0, radius of the undeformed nucleus. ΔR, amplitude of radial deformation. F_n, force applied by myofibrils on the nucleus. L, length between crosslinkers (blue). h, height of a nuclear wrinkle. (**d**) Transversal schematic of a stable nuclear wrinkle (top) and unstable nuclear protrusion (bottom). w, width of a nuclear wrinkle/protrusion. ΔP, difference in hydrostatic pressure between nucleus and wrinkle following an increase of h. (**e**) Model of the stability of wrinkles relative to force on the nucleus. The scaled wrinkle size h/w is plotted as a function of L on the basis of the function $4T/LR_0E$. Above the threshold $h/w \approx 1$, the nucleus is moved to the periphery. Different situations are plotted: relaxed myofibrils (blue), contractile myofibrils (green), contractile myofibrils with predicted nucleus elastic modulus (E) (orange). (**f**) Model for the stability of wrinkles relative to global nuclear stiffness, that is, elastic modulus. The scaled wrinkle size h/w is plotted as a function of global E. The model analyses both large and small E regimes; the intermediate regime is here extrapolated. (**g**) Quantification of peripheral nuclei positioning in 10-day myofibres treated with tetrodotoxin from day 4.5. Data from three independent experiments were combined and error bars represent s.e.m. from indicated n nuclei for each cohort. Unpaired t-test was used to determine statistical significances; $^{***}P < 0.001$. (**h**) Representative images of the first (left) and last (right) frame of a 24-hour time-lapse video of untransfected as well as ChR2-GFP (green)- and H2B-iRFP (red)-transfected myofibres exposed to blue light. Nuclei from transfected (red dashed line) and untransfected (yellow dashed line) myofibres are indicated. 00:00 (hh:mm) corresponds to 3.5-day myofibres. Scale bar, 10 µm. The images shown are representative of four experiments. (**i**) Quantification of nuclei migrating to the periphery as in **b**, and expressing ChR2-GFP not exposed to light. Data from six independent experiments were combined and error bars represent s.e.m. from indicated n nuclei for each cohort. Unpaired t-test was used to determine statistical significances; $^{***}P < 0.001$. Source data are available in Supplementary Table 3.

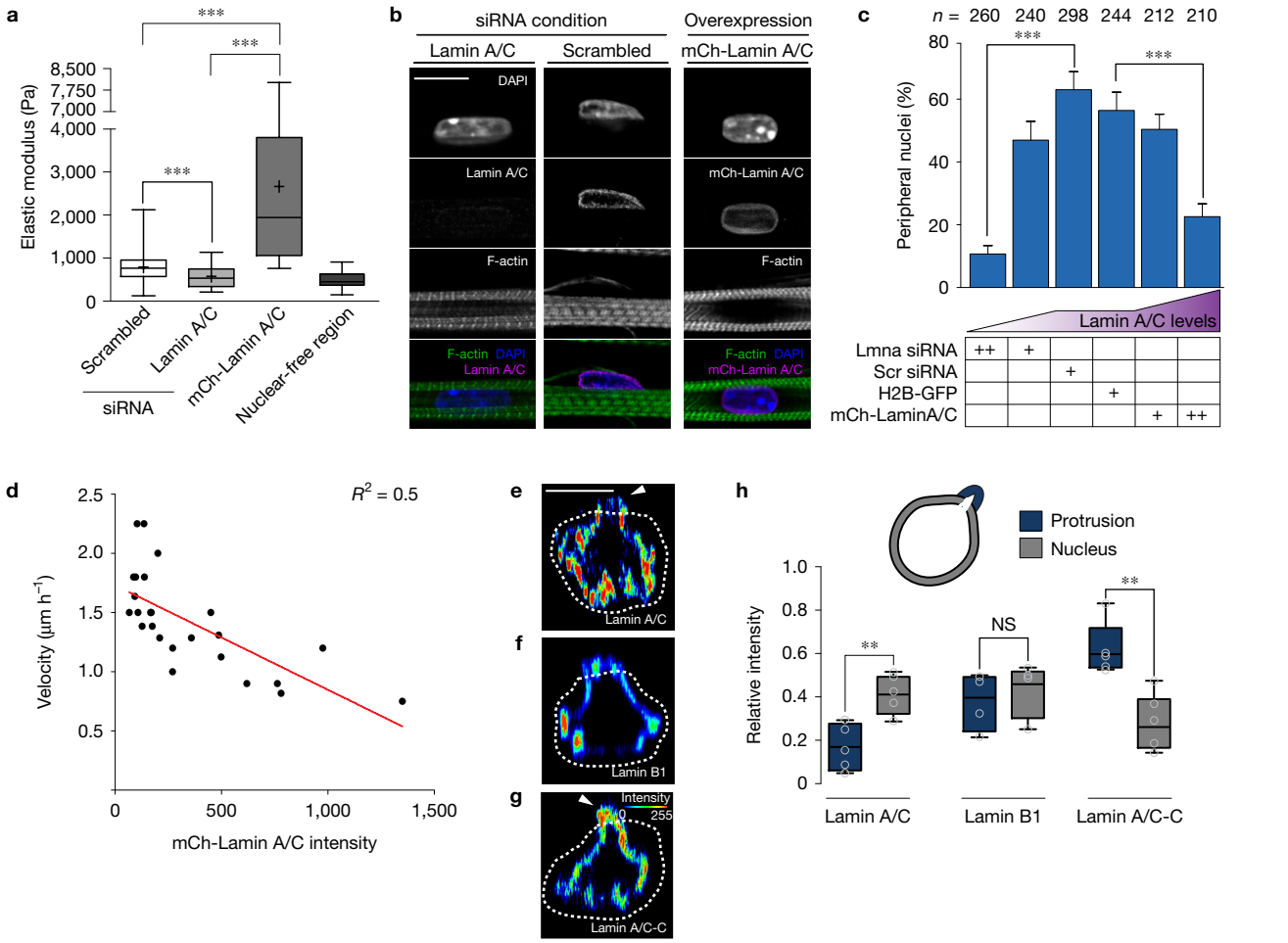

Figure 7 Nuclear stiffness is involved in nuclear movement to the periphery. (**a**) Box plot of nuclear stiffness in 5-day myofibres knocked down for scramble or lamin A/C or transfected with mCh-lamin A/C measured by AFM using a nuclear-free region as a control. Data from four independent experiments were combined and error bars represent s.e.m. from at least 90 measurements for each cohort. Unpaired *t*-test was used to determine statistical significances; $^{***}P<0.001$. Source data are available in Supplementary Table 3. (**b**) Representative immunofluorescence images of 10-day myofibres knocked down for lamin A/C, scrambled or overexpressing mCherry-lamin A/C (mCh-lamin A/C) and stained for lamin A/C (magenta), F-actin (green) and DAPI (nucleus, blue). Scale bar, 10 µm. The images shown are representative of three experiments. (**c**) Quantification of peripheral nuclei positioning in 10-day myofibres knocked down for lamin A/C or scrambled, or overexpressing H2B-mCherry or mCh-lamin A/C. Data from three independent experiments were combined and error bars represent s.e.m. from indicated *n* nuclei for each cohort. Unpaired *t*-test was used to determine statistical significances; $^{***}P<0.001$. Source data are available in Supplementary Table 3. (**d**) Plot correlating velocity of nuclear movement to the periphery with the intensity of the mCh-lamin A/C signal in time-lapse videos of myofibres expressing mCh-lamin A/C between 4.5 and 5.5 days. The red line corresponds to the significant linear regression, $P=0.0001$ of $R^2=0.5004$ for $n=24$ nuclei. Source data are available in Supplementary Table 3. (**e**–**g**) Orthogonal view of nuclei from 5-day myofibres with protrusion initiation, stained for lamin A/C (**e**), lamin B1 (**f**) or lamin A/C-C (**g**). The intensity signal is represented as a heat map. The white dashed line represents the outline of myofibrils. The white arrowheads represent asymmetry in nuclear stiffness. Scale bar, 10 µm. (**h**) Box plot comparing the intensity of lamin A/C, lamin B1 or lamin A/C-C in the part of the nucleus still inside the myofibril bundle (grey, nucleus) versus the forming protrusion (blue, protrusion). Data from five independent experiments were combined and error bars represent s.e.m. from $n=5$ nuclei for each cohort. Unpaired *t*-test was used to determine statistical significances; $^{**}P<0.01$; NS, not significant. The box represents the upper and lower quartile, the bar represents the median and the error bars represent maxima and minima. Source data are available in Supplementary Table 3.

crosslinking (L) induces centripetal forces F_n on the nucleus towards the myofibre axis of the order of $F_n \approx 4TR_0/L$ for each myofibril (Fig. 6b,c). Denoting γ as the surface tension of the nucleus (assumed viscous at the timescale of the experiments), the amplitude of nuclear deformation can be estimated as $\Delta R \approx 4NTR_0/(\gamma L) \approx 0.1$ to 1 µm, where we made use of the effective Young's modulus $E \approx \gamma/R_0$ at low deformation. This results in an increase in the size of the wrinkle, which is between myofibrils, as was experimentally confirmed by 3D time-lapse confocal microscopy and electron microscopy (Supplementary Fig. 6A,B and Supplementary Video 3). As soon as the height h of one of these wrinkles is of the order of its width $2\pi R/N$, the wrinkle is destabilized and forms a protrusion into which all of the nucleus content flows, so that the nucleus finally leaks out of the myofibril bundle (Fig. 6d and Supplementary Fig. 6C). The threshold is given equivalently by $h \approx w$ or $ER_0 = 4T/L$. Given the above orders of magnitude, this threshold is not reached with crosslinking alone (Fig. 6e). To reach the instability threshold, other parameters such as myofibril tension T and elastic modulus (E) must vary[43] (Fig. 6e).

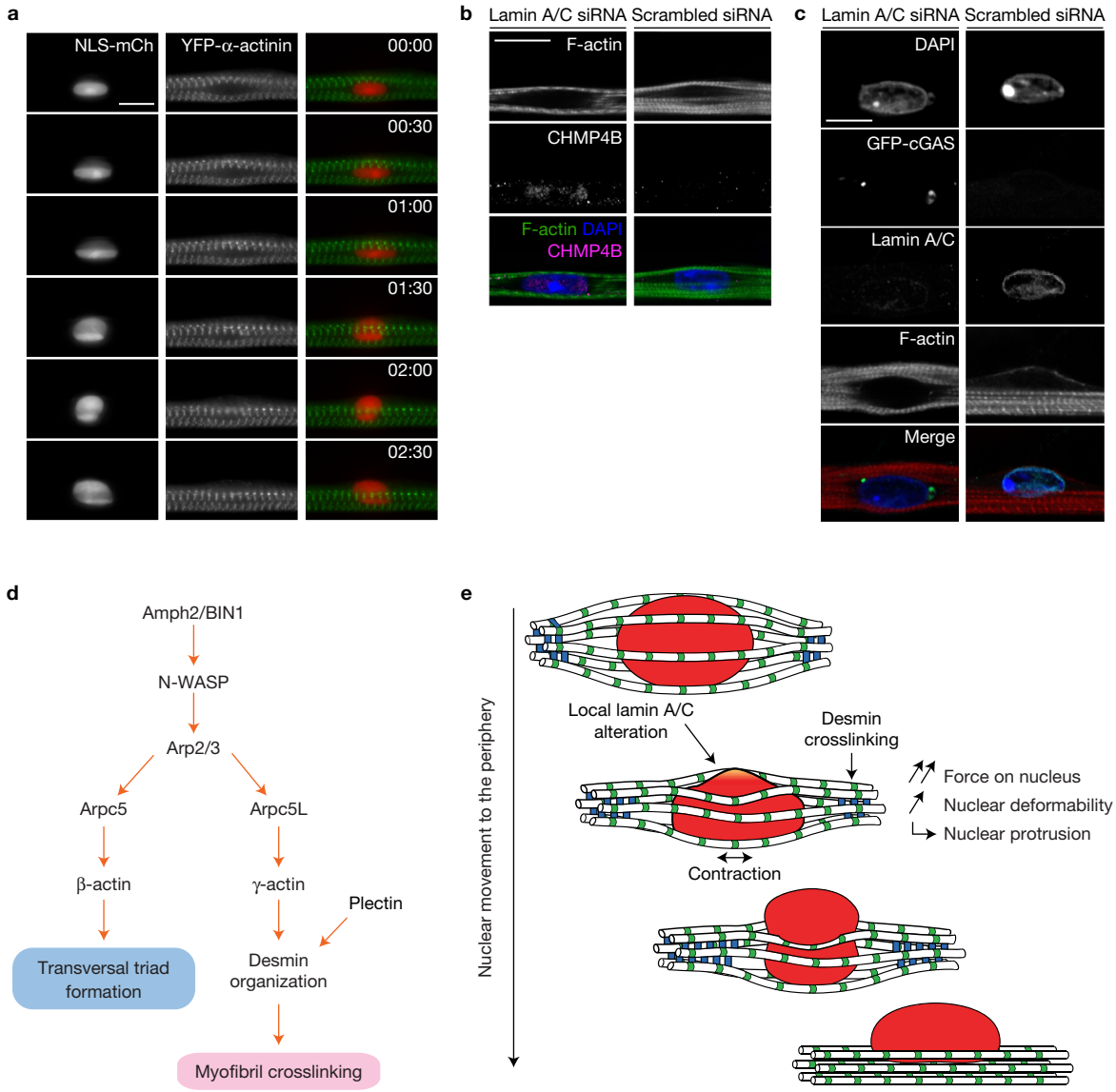

Figure 8 Model of nuclear movement to the periphery in myofibres. (**a**) Kymograph from a time-lapse video of a 4-day myofibre depicting movement to the periphery of a nucleus (NLS-mCh, red) surrounded by myofibrils bundles (YFP-α-actinin, green). Note that NLS-mCh is not released from the nucleus to the cytoplasm, suggesting that nuclear disruption does not occur during nuclear movement to the periphery. Time, hh:mm. Scale bar, 10 μm. (**b**) Representative images of 4.5-day myofibres knocked down for lamin A/C or scrambled and stained for myofibrils (F-actin, green), ESCRT III (CHMP4B, magenta) and nucleus (DAPI, blue). Note that the ESCRT complex is not recruited to the nuclear envelope in the scramble situation. Lamin A/C siRNA was used as a control. Scale bar, 10 μm. The images shown are representative of three experiments. (**c**) Representative images of 10-day myofibres knocked down for lamin A/C or scrambled and transfected with GFP-cGAS (green) as well as being stained for myofibrils (F-actin, red), lamin A/C (cyan) and nucleus (DAPI, blue). Note that GFP-cGAS is not recruited to the nucleus in the scramble situation, suggesting that nuclear disruption does not occur. Lamin A/C siRNA was used as a control. Scale bar, 10 μm. The images shown are representative of three experiments. (**d**) Pathway of the molecular players involved in nuclear movement to the periphery and transversal triad formation. (**e**) Mechanism of nuclear movement to the periphery.

The model also predicts that two adjacent nuclei cannot move to the periphery (Supplementary Fig. 6D), which explains the requirement of nuclei to spread longitudinally before peripheral movement[24].

Myofibril tension T can increase up to 25-fold following contraction, reaching predicted values of $T = 250$ N (Supplementary Fig. 6D)[43]. On the other hand, for the entirety of the nucleus, decreases in elastic modulus E as predicted by the model would enforce large deformations needing an adaptation of the analysis. The nucleus would adopt a cylindrical shape, squeezed between almost undeformed myofibrils. The instability will therefore be reached only for $\gamma < 4NTr_f^3/(R_0^3 L)$, where r_f is the typical radius of the myofibril bundle in the absence of the nucleus. In a situation with large and small E regimes, the instability is not reached with the biophysical parameters of the model. Therefore, the decrease of nuclear stiffness predicted by the theoretical model to be required to reach the instability threshold probably occurs only locally. Thus, peripheral nuclear movement occurs only within a window of nuclear stiffness for the entire nucleus (Fig. 6f).

This theoretical model predicts that alongside myofibril crosslinking, nuclear spreading, myofibre contraction and changes

in nuclear stiffness (globally and locally) play a part in nuclear movement to the periphery.

Nuclear movement requires myofibre contraction

To test the involvement of contraction in nuclear movement, we blocked myofibril contraction with tetrodotoxin and found that peripheral nuclear position is inhibited (Fig. 6g). We also found that optogenetically inducing muscle contraction using ChR2-GFP in premature myofibres (3.5 days) promotes peripheral nuclear movement (Fig. 6h,i and Supplementary Fig. 6E and Supplementary Videos 4 and 5)[44]. Optogenetically induced contractions did not promote nuclear movement in the absence of Arpc5L and γ-actin, although contractions (optogenetically induced and spontaneous) were not impaired (Supplementary Fig. 6F–I). Myofibril contraction is therefore required for peripheral nuclear positioning as predicted by the theoretical model and it is not dependent on Arpc5L or γ-actin.

Nuclear stiffness is important for nuclear movement

The observed nuclear deformation during movement to the periphery and the theoretical model suggest a role for nuclear stiffness in nuclear movement. We manipulated the stiffness of myonuclei either by siRNA-mediated knockdown of lamin A/C (to decrease stiffness) (Supplementary Fig. 7A,B) or by mCherry-lamin A/C (mCh-lamin A/C) overexpression (to increase stiffness), as previously shown[45,46]. Changes in nuclear stiffness following lamin A/C manipulations were directly confirmed by atomic force microscopy (AFM) (Fig. 7a) and by measuring nuclear deformation during optogenetically induced contractions (Supplementary Fig. 7C–E). We found that either the loss or overexpression of lamin A/C decreases the number of peripheral nuclei (Fig. 7b,c and Supplementary Fig. 7F). In contrast the downregulation of lamin B1, which is not involved in nuclear stiffness[45], did not decrease peripheral nuclei (Supplementary Fig. 7G–J). Moreover, re-expression of human mCh-lamin A/C in lamin A/C siRNA-treated myofibres rescued peripheral nuclear positioning (Supplementary Fig. 8A,B). In lamin A/C siRNA-treated myofibres with only one nucleus expressing mCh-lamin A/C, a greater proportion of mCh-lamin A/C nuclei were at the periphery (59%, $n=22$) compared with the lamin A/C-negative nuclei (19.97%, $n=169$) (Supplementary Fig. 8A). Furthermore, the localization of the nuclear envelope proteins Nesprin-1 and SUN2 was not affected by knockdown or overexpression of lamin A/C (Supplementary Fig. 8C,D), demonstrating that the LINC complex nuclear localization is independent of lamin A/C in myofibres. Myofibril integrity was also unaffected by lamin A/C knockdown (Supplementary Fig. 8E). Finally, the levels of overexpressed mCherry-lamin A/C were inversely correlated with the velocity of nuclear movement to the periphery (Fig. 7d). Overall, these data support that variations in nuclear stiffness (decrease or increase) impair nuclear movement as predicted by our theoretical model.

We next investigated whether local alterations of nuclear lamins could be associated with nuclear protrusions as predicted by the model. By observing endogenous lamin A/C and lamin B1 during nuclear movement, we found that lamin A/C, but not lamin B1, is asymmetrically distributed at the nuclear protrusion (Fig. 7e,f,h). Furthermore, a reduction of lamin A/C multimerization, detected with an epitope-specific antibody (lamin A/C-C), also occurs at the nuclear protrusion (Fig. 7g,h)[47]. Despite the lamin A/C asymmetry and the extent of nuclear squeezing, we did not observe nuclear envelope rupture evaluated by leakage of NLS-mCh from the nucleus to the cytoplasm (Fig. 8a), recruitment of the ESCRT complex to the nuclear envelope (Fig. 8b), or recruitment of cGAS from the cytoplasm to the nucleus (Fig. 8c)[48,49]. Our observations thus advocate that nuclear stiffness, dependent on lamin A/C, is locally involved in peripheral nuclear positioning.

DISCUSSION

Nuclear positioning at the periphery of the cell is a hallmark of functional myofibres. Movement of nuclei from a central position to the periphery is a key step during muscle development and is affected in many muscle disorders, as well as muscle regeneration. We elucidate here the mechanism by which myofibres expel their nuclei to the periphery. We demonstrate that this movement is driven by myofibril crosslinking and contraction, and requires a tight regulation of nuclear stiffness by lamin A/C (Fig. 8d). Furthermore, we found that myofibril crosslinking involves the organization of desmin by an Arpc5L-containing Arp2/3 complex together with γ-actin (Fig. 8e).

A mechanism of nuclear positioning at the periphery of myofibres

Nuclear movement within cells is driven by intracellular forces. It has always been reported that the machinery generating these forces is initially polarized to give a direction to the movement[1]. In contrast, the nuclear movement to the periphery of myofibres here described does not involve initial polarized machinery. The forces induced by myofibrils around the nucleus are centripetal and symmetrically distributed around the nucleus. According to our theoretical model and experimental data, the polarization of the movement stems from the formation of a nuclear protrusion that depends on local changes of nuclear stiffness or stochastic alterations of forces exerted by the myofibrils around the nucleus. Thus, the direction of nuclear movement is not only dependent on the cytoplasmic machinery but also on the intrinsic properties of the nucleus. Future work should address whether these local changes in nuclear stiffness are stochastic or locally triggered.

A connection between the nucleus and the cytoskeleton is usually required to drive nuclear movements[8]. This connection is often mediated by the nuclear envelope proteins Nesprins and SUNs (the LINC complex) that link the cytoskeleton to the nuclear lamina[3,5,6]. Our results suggest that a nucleus–cytoskeleton connection is not required for peripheral nuclear movement. Since the LINC complex was implicated in longitudinal spreading of nuclei earlier during myofibre development and anchoring at the plasma membrane, future work should address how the LINC complex is involved in peripheral nuclear positioning[50–55].

Distinct Arp2/3 complexes and actin isoforms have unique roles in skeletal muscle

We also found that distinct populations of Arp2/3 complexes together with specific actin isoforms have segregated functions in skeletal myofibres, nuclear movement and transversal triad formation. Despite having very similar structures, β- and γ-actin isoforms have unique functions in cells, and particularly in skeletal muscle[56–59]. Our results strongly suggest that different physiological functions of β- and γ-actin isoforms can be mediated by specific Arp2/3 complex isoforms[39]. This

specificity can be achieved by compartmentalization of the Arp2/3 and actin complexes, different nucleation activities of Arpc5 isoforms or by different polymerization rates of actin isoforms dependent on Ca^{2+} concentration[33,39,58].

Perinuclear Arp2/3-dependent actin polymerization around the nucleus was found to disrupt nuclear lamina to allow the nuclei of dendritic cells to pass through constrictions during cell migration[60]. Our data suggest that nuclear movement to the periphery occurs by a different mechanism. The Arp2/3 complex and γ-actin are important for the organization of desmin to crosslink myofibrils. Such organization is analogous to the mechanisms found in migrating cells where actin retrograde flow organizes the vimentin intermediate filament cytoskeleton via plectin[34,35]. Desmin replaces vimentin as the main structural intermediate filament during skeletal muscle differentiation. Its organization transitions from a meshwork early on during myofibre development to being organized at the z-line. We show here that the transition of desmin from a meshwork to being organized at the z-line coincides and is required for nuclear movement[18,29–31].

Nuclear positioning in muscle disorders

Muscle disorders such as centronuclear myopathies, myotonic dystrophy, desminopathies and laminopathies exhibit centrally located nuclei[15–17,24,61,62]. Some of the genes encoding the proteins involved in peripheral nuclear positioning are mutated in these disorders. Thus, the mechanism of nuclear positioning described here explains why mutations in apparently diverse proteins leads to a common phenotype of centrally located nuclei in different muscle disorders[16,59,63]. □

METHODS

Methods, including statements of data availability and any associated accession codes and references, are available in the online version of this paper.

Note: Supplementary Information is available in the online version of the paper

ACKNOWLEDGEMENTS

We thank M.-H. Verlhac, M. Dias, J. Pinto, G. Gundersen and S. Tapscott for comments on the manuscript. We thank the Gomes Laboratory for discussions. This work was supported by the European Research Council (E.R.G.), EMBO installation (E.R.G.), the myograd PhD programme (W.R.), AIM France (W.R., B.C., E.R.G.), LISBOA-01-0145-FEDER-007391 co-funded by FEDER through POR Lisboa 2020—Programa Operacional Regional de Lisboa, do PORTUGAL 2020 (E.R.G.), and Fundação para a Ciência e a Tecnologia (E.R.G.). M.W. and J.V.G.A. were supported by the Francis Crick Institute, which receives its core funding from Cancer Research UK (FC001209), the UK Medical Research Council (FC001209) and the Wellcome Trust (FC001209), as well as by postdoctoral fellowships from FRQS (Fonds de recherche du Québec—Santé), EMBO and the Canadian Institutes of Health Research (CIHR) to J.V.G.A.

AUTHOR CONTRIBUTIONS

W.R. carried out experiments and analysed data; J.M. performed lamin- and desmin-related experiments; F.A.C. and N.C.S. carried out AFM experiments. W.R., B.C. and E.R.G. conceived and designed experiments; J.V.G.A. and M.W. provided Arp2/3-related unpublished tools; W.R., R.V. and B.C. designed and executed the physical model; W.R. and E.R.G. wrote the manuscript with assistance from other authors; all authors participated in the critical review and revision of the manuscript.

COMPETING FINANCIAL INTERESTS

The authors declare no competing financial interests.

Published online at http://dx.doi.org/10.1038/ncb3605

1. Gundersen, G. G. & Worman, H. J. Nuclear positioning. *Cell* **152,** 1376–1389 (2013).
2. Horn, H. F. *et al.* The LINC complex is essential for hearing. *J. Clin. Invest.* **123,** 740–750 (2013).
3. Starr, D. A. & Fridolfsson, H. N. Interactions between nuclei and the cytoskeleton are mediated by SUN-KASH nuclear-envelope bridges. *Annu. Rev. Cell Dev. Biol.* **26,** 421–444 (2010).
4. Bolhy, S. *et al.* A Nup133-dependent NPC-anchored network tethers centrosomes to the nuclear envelope in prophase. *J. Cell Biol.* **192,** 855–871 (2011).
5. Starr, D. A. & Han, M. Role of ANC-1 in tethering nuclei to the actin cytoskeleton. *Science* **298,** 406–409 (2002).
6. Crisp, M. Coupling of the nucleus and cytoplasm: role of the LINC complex. *J. Cell Biol.* **172,** 41–53 (2006).
7. Splinter, D. *et al.* Bicaudal D2, Dynein, and Kinesin-1 associate with nuclear pore complexes and regulate centrosome and nuclear positioning during mitotic entry. *PLoS Biol.* **8,** e1000350 (2010).
8. Janota, C. S., Calero-Cuenca, F. J., Costa, J. & Gomes, E. R. SnapShot: nucleo-cytoskeletal interactions. *Cell* **169,** 970 (2017).
9. Almonacid, M. *et al.* Active diffusion positions the nucleus in mouse oocytes. *Nat. Cell Biol.* **17,** 470–479 (2015).
10. Zhao, T., Graham, O. S., Raposo, A. & St. Johnston, D. Growing microtubules push the oocyte nucleus to polarize the *Drosophila* dorsal-ventral axis. *Science* **336,** 999–1003 (2012).
11. Huelsmann, S., Ylänne, J. & Brown, N. H. Filopodia-like actin cables position nuclei in association with perinuclear actin in *Drosophila* nurse cells. *Dev. Cell* **26,** 604–615 (2013).
12. Cadot, B. *et al.* Nuclear movement during myotube formation is microtubule and dynein dependent and is regulated by Cdc42, Par6 and Par3. *EMBO Rep.* **13,** 741–749 (2012).
13. Cadot, B., Gache, V. & Gomes, E. R. Moving and positioning the nucleus in skeletal muscle—one step at a time. *Nucleus* **6,** 373–381 (2015).
14. Metzger, T. *et al.* MAP and kinesin-dependent nuclear positioning is required for skeletal muscle function. *Nature* **484,** 120–124 (2012).
15. Azibani, F., Muchir, A., Vignier, N., Bonne, G. & Bertrand, A. T. Striated muscle laminopathies. *Semin. Cell Dev. Biol.* **29,** 107–115 (2014).
16. Romero, N. B. Centronuclear myopathies: a widening concept. *Neuromuscul. Disord.* **20,** 223–228 (2010).
17. Fugier, C. *et al.* Misregulated alternative splicing of BIN1 is associated with T tubule alterations and muscle weakness in myotonic dystrophy. *Nat. Med.* **17,** 720–725 (2011).
18. Clemen, C. S., Herrmann, H., Strelkov, S. V. & Schröder, R. Desminopathies: pathology and mechanisms. *Acta Neuropathol.* **125,** 47–75 (2013).
19. Clark, K. A., McElhinny, A. S., Beckerle, M. C. & Gregorio, C. C. Striated muscle cytoarchitecture: an intricate web of form and function. *Annu. Rev. Cell Dev. Biol.* **18,** 637–706 (2002).
20. Fuchs, E. & Weber, K. Intermediate filaments: structure, dynamics, function and disease. *Annu. Rev. Biochem.* **63,** 345–382 (1994).
21. Lowery, J., Kuczmarski, E. R., Herrmann, H. & Goldman, R. D. Intermediate filaments play a pivotal role in regulating cell architecture and function. *J. Biol. Chem.* **290,** 17145–17153 (2015).
22. Al-Qusairi, L. & Laporte, J. T-tubule biogenesis and triad formation in skeletal muscle and implication in human diseases. *Skelet. Muscle* **1,** 26 (2011).
23. Flucher, B. E., Takekura, H. & Franzini-Armstrong, C. Development of the excitation-contraction coupling apparatus in skeletal muscle: association of sarcoplasmic reticulum and transverse tubules with myofibrils. *Dev. Biol.* **160,** 135–147 (1993).
24. Falcone, S. *et al.* N-WASP is required for Amphiphysin-2/BIN1-dependent nuclear positioning and triad organization in skeletal muscle and is involved in the pathophysiology of centronuclear myopathy. *EMBO Mol. Med.* **6,** 1455–1475 (2014).
25. Egile, C. *et al.* Activation of the Cdc42 effector N-Wasp by the *Shigella flexneri* Icsa protein promotes actin nucleation by Arp2/3 complex and bacterial actin-based motility. *J. Cell Biol.* **146,** 1319–1332 (1999).
26. Machesky, L. M. *et al.* Scar, a WASp-related protein, activates nucleation of actin filaments by the Arp2/3 complex. *Proc. Natl Acad. Sci. USA* **96,** 3739–3744 (1999).
27. Yarar, D., To, W., Abo, A. & Welch, M. D. The Wiskott–Aldrich syndrome protein directs actin-based motility by stimulating actin nucleation with the Arp2/3 complex. *Curr. Biol.* **9,** 555–558 (1999).
28. Pimentel, M. R., Falcone, S., Cadot, B. & Gomes, E. R. *In vitro* differentiation of mature myofibers for live imaging. *J. Vis. Exp. JoVE* http://dx.doi.org/10.3791/55141 (2017).
29. Ralston, E. *et al.* Blood vessels and desmin control the positioning of nuclei in skeletal muscle fibers. *J. Cell. Physiol.* **209,** 874–882 (2006).
30. Li, Z. *et al.* Desmin is essential for the tensile strength and integrity of myofibrils but not for myogenic commitment, differentiation, and fusion of skeletal muscle. *J. Cell Biol.* **139,** 129–144 (1997).
31. Milner, D. J., Weitzer, G., Tran, D., Bradley, A. & Capetanaki, Y. Disruption of muscle architecture and myocardial degeneration in mice lacking desmin. *J. Cell Biol.* **134,** 1255–1270 (1996).
32. Dugina, V., Zwaenepoel, I., Gabbiani, G., Clément, S. & Chaponnier, C. β- and γ-cytoplasmic actins display distinct distribution and functional diversity. *J. Cell Sci.* **122,** 2980–2988 (2009).

33. Bergeron, S. E., Zhu, M., Thiem, S. M., Friderici, K. H. & Rubenstein, P. A. Ion-dependent polymerization differences between mammalian β- and γ-nonmuscle actin isoforms. *J. Biol. Chem.* **285,** 16087–16095 (2010).
34. Dupin, I., Sakamoto, Y. & Etienne-Manneville, S. Cytoplasmic intermediate filaments mediate actin-driven positioning of the nucleus. *J. Cell Sci.* **124,** 865–872 (2011).
35. Jiu, Y. *et al.* Bidirectional interplay between vimentin intermediate filaments and contractile actin stress fibers. *Cell Rep.* **11,** 1511–1518 (2015).
36. Korobova, F. & Svitkina, T. Arp2/3 complex is important for filopodia formation, growth cone motility, and neuritogenesis in neuronal cells. *Mol. Biol. Cell* **19,** 1561–1574 (2008).
37. Gournier, H., Goley, E. D., Niederstrasser, H., Trinh, T. & Welch, M. D. Reconstitution of human Arp2/3 complex reveals critical roles of individual subunits in complex structure and activity. *Mol. Cell* **8,** 1041–1052 (2001).
38. Nolen, B. J. *et al.* Characterization of two classes of small molecule inhibitors of Arp2/3 complex. *Nature* **460,** 1031–1034 (2009).
39. Abella, J. V. G. *et al.* Isoform diversity in the Arp2/3 complex determines actin filament dynamics. *Nat. Cell Biol.* **18,** 76–86 (2016).
40. Konieczny, P. *et al.* Myofiber integrity depends on desmin network targeting to Z-disks and costameres via distinct plectin isoforms. *J. Cell Biol.* **181,** 667–681 (2008).
41. Goldspink, G. The proliferation of myofibrils during muscle fibre growth. *J. Cell Sci.* **6,** 593–603 (1970).
42. Yoshikawa, Y., Yasuike, T., Yagi, A. & Yamada, T. Transverse elasticity of myofibrils of rabbit skeletal muscle studied by atomic force microscopy. *Biochem. Biophys. Res. Commun.* **256,** 13–19 (1999).
43. Colomo, F., Piroddi, N., Poggesi, C., Te Kronnie, G. & Tesi, C. Active and passive forces of isolated myofibrils from cardiac and fast skeletal muscle of the frog. *J. Physiol.* **500,** 535–548 (1997).
44. Sakar, M. S. *et al.* Formation and optogenetic control of engineered 3D skeletal muscle bioactuators. *Lab. Chip* **12,** 4976–4985 (2012).
45. Lammerding, J. *et al.* Lamins A and C but not Lamin B1 regulate nuclear mechanics. *J. Biol. Chem.* **281,** 25768–25780 (2006).
46. Swift, J. *et al.* Nuclear Lamin-A scales with tissue stiffness and enhances matrix-directed differentiation. *Science* **341,** 1240104 (2013).
47. Ihalainen, T. O. *et al.* Differential basal-to-apical accessibility of lamin A/C epitopes in the nuclear lamina regulated by changes in cytoskeletal tension. *Nat. Mater.* **14,** 1252–1261 (2015).
48. Denais, C. M. *et al.* Nuclear envelope rupture and repair during cancer cell migration. *Science* **352,** 353–358 (2016).
49. Raab, M. *et al.* ESCRT III repairs nuclear envelope ruptures during cell migration to limit DNA damage and cell death. *Science* **352,** 359–362 (2016).
50. Apel, E. D., Lewis, R. M., Grady, R. M. & Sanes, J. R. Syne-1, a dystrophin- and Klarsicht-related protein associated with synaptic nuclei at the neuromuscular junction. *J. Biol. Chem.* **275,** 31986–31995 (2000).
51. Espigat-Georger, A., Dyachuk, V., Chemin, C., Emorine, L. & Merdes, A. Nuclear alignment in myotubes requires centrosome proteins recruited by nesprin-1. *J. Cell Sci.* **129,** 4227–4237 (2016).
52. Grady, R. M., Starr, D. A., Ackerman, G. L., Sanes, J. R. & Han, M. Syne proteins anchor muscle nuclei at the neuromuscular junction. *Proc. Natl Acad. Sci. USA* **102,** 4359–4364 (2005).
53. Wilson, M. H. & Holzbaur, E. L. F. Nesprins anchor kinesin-1 motors to the nucleus to drive nuclear distribution in muscle cells. *Development* **142,** 218–228 (2015).
54. Zhang, X. *et al.* Syne-1 and Syne-2 play crucial roles in myonuclear anchorage and motor neuron innervation. *Development* **134,** 901–908 (2007).
55. Lei, K. *et al.* SUN1 and SUN2 play critical but partially redundant roles in anchoring nuclei in skeletal muscle cells in mice. *Proc. Natl Acad. Sci. USA* **106,** 10207–10212 (2009).
56. Belyantseva, I. A. Gamma-actin is required for cytoskeletal maintenance but not development. *Proc. Natl Acad. Sci. USA* **106,** 9703–9708 (2009).
57. Prins, K. W., Call, J. A., Lowe, D. A. & Ervasti, J. M. Quadriceps myopathy caused by skeletal muscle-specific ablation of βcyto-actin. *J. Cell Sci.* **124,** 951–957 (2011).
58. Gokhin, D. S. & Fowler, V. M. Cytoplasmic γ-actin and tropomodulin isoforms link to the sarcoplasmic reticulum in skeletal muscle fibers. *J. Cell Biol.* **194,** 105–120 (2011).
59. Sonnemann, K. J. *et al.* Cytoplasmic γ-actin is not required for skeletal muscle development but its absence leads to a progressive myopathy. *Dev. Cell* **11,** 387–397 (2006).
60. Thiam, H.-R. *et al.* Perinuclear Arp2/3-driven actin polymerization enables nuclear deformation to facilitate cell migration through complex environments. *Nat. Commun.* **7,** 10997 (2016).
61. Zwerger, M. *et al.* Myopathic lamin mutations impair nuclear stability in cells and tissue and disrupt nucleo-cytoskeletal coupling. *Hum. Mol. Genet.* **22,** 2335–2349 (2013).
62. Hnia, K. *et al.* Myotubularin controls desmin intermediate filament architecture and mitochondrial dynamics in human and mouse skeletal muscle. *J. Clin. Invest.* **121,** 70–85 (2011).
63. Goldfarb, L. G. & Dalakas, M. C. Tragedy in a heartbeat: malfunctioning desmin causes skeletal and cardiac muscle disease. *J. Clin. Invest.* **119,** 1806–1813 (2009).

DOI: 10.1038/ncb3605

METHODS

Cell culture, animals, transfections and reagents. All procedures using animals were approved by the Institutional ethics committee and followed the guidelines of the National Research Council Guide for the care and use of laboratory animals. *In vitro* myofibres were generated with primary myoblasts isolated from 5–7-day-old pups of C57BL/6 mice, using the protocol previously described[64]. Cells were grouped regardless of gender. *In vivo* clearing and myofibre isolation was performed on newborn mice.

Cells were transfected with siRNA (20 nM) using RNAiMAX (cat. no. 15338-100), cDNA 1 μg μl^{-1} using Lipofectamine-LTX Plus reagent (cat. no. 13778-150) or using Lipofectamine 2000 (cat. no. 11668-019) following the manufacturer's instructions (Life Technologies, see individual catalogue numbers). For primary myoblasts, cells were transfected 6 h prior to differentiation to promote protein silencing or overexpression effectiveness from the beginning of differentiation.

CK666 (Arp2/3 inhibitor) was obtained from Sigma (cat. no. SML0006-5MG) and was added to 4.5-day myofibres at a concentration of 50 μM. Tetrodotoxin (contraction inhibitor) was obtained from Sigma (cat. no. T8024) and was added to 4.5-day myofibres at a concentration of 10 μM.

Plasmids. pcDNA GFP was a gift from A. Gautreau (Ecole Polytechnique de Palaiseau, France). GFP-Arpc5 and GFP-Arpc5L were previously described[65]. The γ-actin mouse cDNA, synthesized from Life Technologies with silent point mutations to make it resistant against siRNA, was cloned into a pDONR221 Gateway entry vector (Life Technologies) and recombined into a pEGFP_C1-GW destination vector and a pRFP-GW destination vector to generate pEGFP_C1- γ-actin and pRFP-γ-actin plasmids respectively. The β-actin cDNA, synthesized from Life Technologies with silent point mutations to make it resistant against siRNA, was cloned into a pDONR221 Gateway entry vector (Life Technologies) and recombined into a pEGFP-C1-GW destination vector and a pRFP-GW destination vector to generate a pEGFP_C1-β-actin and pRFP-β-actin plasmids respectively. The ChR2-GFP construct was obtained through Addgene (plasmid no. 20939). YFP-α-actinin plasmid was a gift from P. Lappalainen (University of Helsinki, Finland). iRFP-H2B was a gift from M. Coppey (Institut Curie, France). EmGFP-Desmin was obtained through Addgene (plasmid no. 54059). NLS-tdtomato, H2B-mCherry was a gift from the Lammerding laboratory (Weill Institute, USA). GFP-CGas was a gift from the Piel laboratory (Institut Curie, France).

Antibodies. Antibody information is provided in Supplementary Table 1.

siRNA. The sequences of siRNAs used in the study are provided in Supplementary Table 2.

Western blotting. Cells were lysed in PBS + 1%SDS and passed through a Qiashredder column (Qiagen) to disrupt DNA. Protein concentration was measured with a BCA kit according to the manufacturer's instructions (Pierce). Equal amounts of sample were boiled in 30 μl sample buffer and were loaded onto 4–12% pre-cast Bis-Tris gel (Invitrogen) and transferred into nitrocellulose membrane using the iBlot apparatus (Invitrogen). Membranes were blocked with blocking buffer (5% non-fat dry milk, 0.1% Tween in TBS). Primary antibodies were incubated overnight in blocking buffer at 4 °C. After three washes with TBS-Tween 0.1%, membranes were incubated with HRP-conjugated secondary antibodies (1 h at room temperature). Proteins were visualized using ECL reagent (Pierce). All western blots were performed three times.

Immunoprecipitation. For immunoprecipitation of GFP-tagged proteins, a GFP-Trap system (Chromotek cat. no. gtm-20) was used following the manufacturer's instructions. After thorough washing with the lysis buffer, bound proteins were eluted in sample buffer, boiled and analysed by western blot.

Immunofluorescence and immunohistochemistry. Fluorodishes were fixed in 4% paraformaldehyde for 10 min, permeabilized with Triton X-100 (0.5% in PBS) and aspecific sites were blocked with BSA 1% and goat serum 10% for 30 min. Primary antibodies were added overnight at 4 °C in saponin 0.1% and BSA 1% in PBS. Fluorodishes or fibres were washes three times and then incubated with secondary antibodies together with DAPI for 60 min. Each experiment was performed at least three times.

Lamin quantifications of nuclear positioning. Variability in the strength of the lamin A/C knockdown could be observed by immunofluorescence. As such, myofibres were quantified with either complete knockdown (referred as '++') or partial knockdown (referred as '+'). This allowed a quantification of varying levels of lamin A/C and therefore nuclear stiffness. From the Lmna siRNA experiments, when lamin A/C intensity was below 10% of the control intensity, it was categorized as '++' knockdown. When lamin A/C intensity was between 10% and 50% of the control intensity, it was categorized as '+' knockdown. For the overexpression experiments, we normalized mCh-lamin A/C expression relative to the higher-expressing mCh-Lamin A/C nucleus (which was 100%). When intensities were between 100% and 50%, the intensity was categorized as '++' overexpression. When intensities were below 50%, the intensity was categorized as '+'.

Isolation of myofibres. TA single fibres were isolated as described previously[64]. TA muscle was explanted from newborn male or female CD1 mice and then digested in DMEM containing 0.2% type I collagenase (Sigma) for 2 h at 37 °C. Mechanical dissociation of fibres was performed using a thin Pasteur pipette and followed under a transilluminating-fluorescent stereomicroscope.

Atomic force microscopy. The elasticity of the cells was measured using an atomic force microscope NanoWizard II (JPK Instruments) mounted on the top of an Axiovert 200 inverted microscope (Carl Zeiss). Nanoindentation experiments were carried out on live cells, at 25 °C, in Iscove's modified Dulbecco's media (IMDM). For these measurements, non-functionalized OMCL TR-400-type (Olympus, Japan) with a long triangular cantilever and a silicon nitride tips (nominal force constant of 20 pN nm^{-1}) (Olympus) were used. Differential interference contrast (DIC) microscopy and fluorescence microscopy were used to position the tip on the top of the cell nucleus of each cell previously transfected. For every contact between cell and cantilever, the distance between the cantilever and the cell was adjusted to maintain a maximum applied force of 500 pN before retraction. Cell elasticity was measured on one point of each cell adhered to the tissue culture dish (eight force–distance curves per cell), and on approximately eight cells of three different culture dishes. A total of 24 cells were tested for each experimental condition. Data collection for each force–distance cycle was performed at 2 Hz and with a z-displacement range of 8 μm. Nuclear-free regions were used as a comparative control to account for membrane and organelle stiffness. Data acquired on the nanoindentation experiments (force indentation curves) were analysed to obtain the cells Young's modulus (E), using JPK Image Processing v. 5.1.8, by the application of the Hertzian model. The probe was modelled as a quadratic pyramid, with a tip angle of 35° (half-angle to face) and a Poisson ratio of 0.50.

Fluorescence recovery after photobleaching. Fluorescence recovery after photobleaching experiments were performed on a Zeiss LSM 880 confocal microscope from Carl Zeiss equipped with the ZEN grey edition software, using a Plan-Apochromat 63× Oil DIC objective (numerical aperture: 1.40). Each fibre was imaged during 5 min periods at 5 s intervals, with two frames being acquired before bleaching. Fluorescence bleaching was conducted using a 488 nm wavelength laser at 100% laser power (maximum laser power) for 20 iterations. The bleached area consisted of a circle with the average width of myofibres. Fluorescence intensities of the bleached regions were obtained using FIJI software and a nonlinear one-phase association curve available in Graphpad Prism was used for data fitting. Data analysis was performed in Microsoft Excel and Graphpad Prism, and the data were averaged for at least eight cells for each of the conditions studied.

Transmission electron microscopy. Myofibres were fixed for 1 h at 4 °C in 0.1 M sodium cacodylate buffer, pH 7.3, containing 2.5% (v/v) gluteraldehyde and 0.1% (v/v) formaldehyde. Samples were incubated for 1 h on ice in 1% (aq.) osmium tetroxide and 30 min block in 1% (aq.) uranyl acetate. Dehydration was performed using an ethanol gradient (50–70–95–100%). Samples were flat embedded in Durcupan resin and hardened at 60 °C for 72 h. For cells in the transversal plane (top to bottom of the cell), sections were directly obtained, and for the coronal plane of orientation (anterior to posterior) two blocks of the same condition were glued together and sectioned in a 90° plane in relation to the flat surface of the blocks; both orientations were sectioned using an ultramicrotome Reichert Supernova (Leica Microsystems); semi-thin sections (500 nm) were stained with toluidine blue for light-microscope evaluation. Ultrathin sections (70 nm) were obtained and collected in Formvar-coated copper slot grids (AGAR Scientific), and counter-stained with uranyl acetate and lead citrate (Reynold recipe); regions of interest in both orientation planes were sequentially screened in a Hitachi H-7650 transmission electron microscope at 100 kV acceleration.

Whole-muscle clearing. Tissue clearing is a method to clarify the tissue to replace the dehydrant with a miscible agent[66]. The tissue will therefore become translucent for greater 3D imaging. Legs of newborn mice were isolated and fixed overnight in PFA 4%. Legs were pre-treated overnight with (1% Triton, 0.5% Tween, 0.25% NP-40, 0.25% Na-deoxycholate, 3% BSA, 0.002% Na azide, 1% urea in PBS). The following day, legs were incubated in CBB before being incubated with primary antibody for two days. After primary antibody incubation, legs were washed several time with PBT and washed overnight with rotation. The following day, legs were incubated with secondary antibody for two days and then washed with PBT several

times and overnight. DAPI was subsequently added for 3 h and washed several times before starting the clearing treatment. Clearing began by incubating legs with 25% formamide and 10% PEG for an hour, followed by 50% formamide and 20% PEG for an hour and finishing with 50% formamide and 20% PEG overnight. Legs were then mounted with fluoromount and imaged.

Peripheral nuclei position quantification. Quantification was performed as previously described[64]. Briefly, myofibres were stained for DAPI and traids and images in Z-stacks with 0.5 mm interval were acquired with a Leica SPE confocal microscope with a 63 × 1.3 NA Apo objective. Nuclei extruding the myofibre periphery were scored as peripheral.

Transversal triad quantification. Quantification was performed as previously described[64]. Briefly, myofibres were stained for DHPR1, triadin and DAPI and images in Z-stacks with 0.5 mm interval were acquired with a Leica SPE confocal microscope with a 63 × 1.3 NA Apo objective. Myofibres having more than 50% of triads organized, where DHPR and Triadin were transversally overlapping, were scored as positive.

Protrusion intensity quantification. Orthogonal images of nuclear buds were generated and line scans were drawn on the nuclear envelope either on part of the nucleus still inside the myofibril bundle or part of the nucleus outside the bundle (bud). For Supplementary Fig. 2, line scans were drawn on the bud in contact with the plasma membrane (cap) and the bud that was not (side). Line scan width was 1 µm.

Line scans. A line scan was drawn at the same spot in the kymograph depicting desmin and a plot was generated. Line scan width was 2 µm.

Microscopy. Live imaging was performed using an incubator to maintain cultures at 37 °C and 5% CO_2 (Okolab) and ×20 0.3 NA PL Fluo dry objective. Epi-fluorescence images were acquired using a Nikon Ti microscope equipped with a CoolSNAP HQ2 camera (Roper Scientific), and an XY-motorized stage (Nikon), driven by Metamorph (Molecular Devices). Confocal images were acquired using a Leica SPE confocal microscope with a 63× 1.3 NA Apo objective or Zeiss LSM 710 and Zeiss LSM 880 with a 63× 1.4 NA Plan-Apochromat objective. Three-dimensional time-lapse spinning-disc microscopy was performed using a Zeiss Cell Observer Spinning Disk system equipped with Z-piezo (Prior), Spinning Disk CSU-X1M 5000 (Yokogawa), 488 nm 561 nm and 638 nm excitation laser, an incubator to maintain cultures at 37 °C and 5% CO_2 (Pekon), an electron-multiplying CCD (charge-coupled device) camera Evolve 512 (Photometrics) and a 63× 1.4 NA Plan-Apochromat objective. Fiji was used as an imaging processing software and Adobe Illustrator was used to raise figures.

Area around the nucleus quantification. Images from the middle plane of a z-stack expressing YFP-α-actinin and H2B-iRFP, obtained with spinning-disc microscopy were used. One transversal line was drawn at a distance of 30 µm on each side of the nucleus. The dark area on each side of the nucleus between this line, the myofibrils and the nucleus was measured using Fiji. These measurements were performed in time-lapse images. Values were normalized relative to the first time point.

Percentage of nucleus at the periphery. During nuclear movement to the periphery, area of nuclei emerging from the myofibre and total area of the nucleus were assessed. A ratio was obtained and a percentage was calculated over time.

Spontaneous contraction quantifications. Five-day myofibres were monitored under a light microscope with phase contrast. Contracting myofibres were spotted and the number of contractions was monitored over a one-minute duration to determine contraction frequency.

Spherical and volumetric assessment. Time-lapse images were reconstructed in 3D and over time using the software Imaris and surface three-dimensional rendering was performed. Spherical and volumetric values were extracted from the 3D render of nuclei at each time point. The rendering was adapted for each time point to the background to retain fluorescence intensity. Sphericity was calculated as defined in 1932[67]. Values were normalized relative to the first time point. Sphericity and volume were measured every 5 min and normalized to the first point for Fig. 2a,b.

Laser ablation and bleaching. Myofibres of 4.5 days were incubated in a Zeiss LSM 880 microscope at 37 °C and 5% CO_2. Five circles were drawn on both sides of nuclei as ROIs to be ablated or bleached. A Diode 405-30 laser was used at 100% (maximum power 30 mW) with a scan speed of 3, and three iterations for ablation and an argon laser was used at 50% (maximum power 25 mW) with a scan speed of 3 and three iterations for bleaching. Five minutes after ablation or bleaching, cells were acquired in z for 3D reconstruction to analyse volume and sphericity.

Nuclear deformations during contractions. Myofibres of 4.5 days were incubated at 37 °C and 5% CO_2 in the Zeiss Cell Observer Spinning Disk system. Myofibres were transfected with the optogenetic channel ChR2 and NLS-mCherry or mCherry-lamin A/C as well as knocked down for scramble or lamin A/C. Videos were acquired in stream mode in the 555 channel and blue light was shone on cells at different intervals during acquisition to induce contraction. Nuclei length was then measured between relaxed and contracted state and normalized on myofibre thickness.

Pausing duration quantifications. Nuclear movement velocity along myofibres was calculated using software ICY. Nuclei were considered pausing when they moved less than 0.0015 µm s^{-1} for a minimum time of an hour. The cutoff value for nuclear pausing (one hour at less than 0.0015 µm s^{-1}) was chosen on the basis of visual correlation between nuclear movement and pausing from live imaging videos.

Model. The nucleus of radius $R_0 \approx 6\,\mu m$ (at rest) has a complex rheology. It is often described as a linear elastomer (Young's modulus $E \approx 1$ to 10 kPa), whose elastic component is largely due to the lamina envelope. However, for large and slow deformations a viscous behaviour is expected, as suggested in other contexts[68]. The effective surface tension of the nucleus in a skeletal muscle cell can therefore be estimated as $\gamma \approx R_0 E$. Before peripheral movement, the nucleus is wrapped by a bundle of $N \approx 30$ myofibrils and centred along the symmetry axis of the bundle. We assume that each myofibril can be modelled as an active spring, whose passive tension ($T \approx 1$ to 10 nN) was assessed using 2.7 µm sarcomere length (empirical measurement).

During peripheral migration of the nucleus to the periphery, we assume that myofibrils are crosslinked together through Arpc5L-containing Arp2/3 complexes and γ-actin (with a typical distance between myofibrils of the order of 1 µm) and with a distance $L \approx 30\,\mu m$ between crosslinking points along the myofibre. This induces a normal force F_n on the nucleus towards the myofibre axis of the order of $F_n \approx 4TR_0/L$ for each myofibril. This force first induces a global deformation of the nucleus, which elongates along the myofibre axis. The deformation can be estimated by balancing the surface energy cost of a deformation of amplitude ΔR of the nucleus, which is $dE_s \approx \gamma \Delta R^2$, and the work of the total normal force exerted by myofibrils given by $dW \approx NF_n \Delta R$. This yields $\Delta R \approx 4NT/(LE) \approx 0.1$–1 µm, which is consistent with observations.

Such conformation of the nucleus squeezed by myofibrils is unstable. Between each myofibril squeezing a wrinkle can form. We now argue that as soon as the height h of one of these wrinkles is of the order of its width $2\pi R/N$, the wrinkle is destabilized forming a bleb and all of the nucleus content flows into the bleb, so that the nucleus is expelled out of the bundle. Let us denote by ΔP the difference of hydrostatic pressure between the inside and outside of the nucleus. Laplace law gives $\Delta P = \gamma C$, where C is the mean curvature of a wrinkle. For $h < 2\pi R/N$, an increase of the wrinkle height h locally increases the curvature C, leading to a local increase in the hydrostatic pressure in the wrinkle, which subsequently relaxes. Conversely, for $h > 2\pi R/N$, an increase of h reduces the curvature C, thereby leading to a decrease in the local hydrostatic pressure in the wrinkle. The nucleoplasm subsequently flows into the wrinkle, which is henceforth destabilized and leads to bleb formation. The threshold of this instability is reached when $\gamma R_0 \approx 4TR_0/L$, or $T > ER_0L/4$; this condition is obtained by balancing normal forces on a myofibril for $h \approx 2\pi R/N$: the normal force induced by the myofibrils is $4TR_0/L$, while the restoring force induced by the deformed nucleus is of the order γR_0 when $h = 2\pi R/N$. Note that here we assumed a constant surface tension γ following deformation, which yields a threshold independent of the number of myofibrils. Given the above orders of magnitude, this threshold can be reached in principle, provided that tension takes large values and Young's modulus E is locally small enough values. This shows that such a mechanism of nucleus off-centring may indeed be at work. In particular, this mechanism shows that the motion of the nucleus to the periphery is favoured by an increased tension of myofibrils and a reduced distance between crosslinkers.

When the surface tension is low (that is, at low level of lamin A/C), the nucleus undergoes large deformations and this analysis needs to be adapted. One finds that a cylindrical shape of the nucleus, squeezed between almost undeformed myofibrils, is stable for $\gamma < 4NTr_f^3/(R_0^3 L)$, where r_f is the typical radius of the myofibril bundle in the absence of nucleus. Altogether, this shows that the mechanism of positioning of the nucleus to the periphery is efficient only within a window of values of nucleus rigidity (here modelled effectively as a surface tension), which is controlled by lamin A/C levels.

Optogenetically induced contraction. Myofibres were transfected with the ChR2-GFP and iRFP-H2B constructs. Following blue-light exposure, the ChR2 channel opens to become permeable to Na^+ ions. This induces a depolymerization of the membrane and a subsequent contraction of the myofibre. To monitor the effect of contraction on peripheral nuclear localization, 3.5-day myofibres were exposed to 100 ms of blue light using a bandpass filter 470/40 every 10 min for 24 h. Bright-field and epifluorescent images were acquired every 10 min. The number of

DOI: 10.1038/ncb3605

peripheral nuclei positioned over a period of 24 h was assessed both in transfected and untransfected myofibres. Peripheral nuclei were scored when more than a quarter of the total size of nuclei protruded from the membrane. A ratio of nuclei having reached the periphery over total nuclei assessed was obtained and a percentage calculated.

Correlative velocity of nuclei and lamin A/C expression. Time-lapse videos of myofibres overexpressing mCherry-lamin A/C were analysed by quantifying the overall intensity of nuclei expressing the construct and the time required to reach the periphery (20 min per frame). The intensity of lamin A/C was obtained by measuring the integrated fluorescence density, which is the sum of all the pixels, which equals the product of area and mean grey value, subtracted by the background integrated density.

Statistics and reproducibility. Statistical analysis was performed with Graphpad Prism (version 5.0 of GraphPad Software). Pair-wise comparisons were made with Student's *t*-test. In peripheral nuclei positioning analysis and in fibre thickness analysis in myofibres, Student's *t*-tests were performed between scramble siRNA and experimental condition. For biochemical experiments using human samples, statistical analysis was performed using the Mann–Whitney *U*-test, Wilcoxon matched-pairs signed ranked test or the unpaired Student's test and multiple statistical comparisons between samples were performed by two-way analysis of variance followed by a Bonferroni's *t*-test *post hoc* correction to obtain a better evaluation of the variability between samples from the same group and samples from each compared group and statistical significance was set at $^{*}P < 0.05$. The distribution of data points is expressed as mean ± s.e.m. from three or more independent experiments. For statistics with an *n* lower than 10, a statistical power test was performed using GPower 3.1 on the basis of the statistical test used. Outliers were detected using Grubb's test at a P value <0.05. Variability arises in the maturity obtained from the *in vitro* muscle system obtained from primary myoblasts. As such, a minimum of 55% of peripheral nuclei in the control cohorts were required to consider the experiment. Representative images are from at least three experiments, except for *in vivo* clearing and myofibre isolation, which are from two experiments. All blots were produced at least three times.

Code availability. Image processing was performed using Fiji. Sphericity and volume of nuclei during movement to the periphery was done using Imaris. Algorithms can be obtained at the following link: http://www.bitplane.com/resources.aspx.

Data availability. Source data for Figs 2a,b, 2d,f–g, 3b,e, 4c,g, 5f, 6i and 7a,c,d,h as well as Supplementary Figs Supplementary Figs 1B,C, 2E, 3F,G, 4E,G, 5D,H, 6F, 7D–F,J and 8B are available in Supplementary Table 3. All other data supporting the findings of this study are available from the corresponding author on reasonable request.

64. Falcone, S. *et al.* N-WASP is required for Amphiphysin-2/BIN1-dependent nuclear positioning and triad organization in skeletal muscle and is involved in the pathophysiology of centronuclear myopathy. *EMBO Mol. Med.* **6,** 1455–1475 (2014).
65. Abella, J. V. G. *et al.* Isoform diversity in the Arp2/3 complex determines actin filament dynamics. *Nat. Cell Biol.* **18,** 76–86 (2016).
66. Richardson, D. S. & Lichtman, J. W. Clarifying tissue clearing. *Cell* **162,** 246–257 (2015).
67. Wadell, H. Volume, shape, and roundness of rock particles. *J. Geol.* **40,** 443–451 (1932).
68. Thiam, H.-R. *et al.* Perinuclear Arp2/3-driven actin polymerization enables nuclear deformation to facilitate cell migration through complex environments. *Nat. Commun.* **7,** 10997 (2016).

nature cell biology

DOI: 10.1038/ncb3605

In the format provided by the authors and unedited.

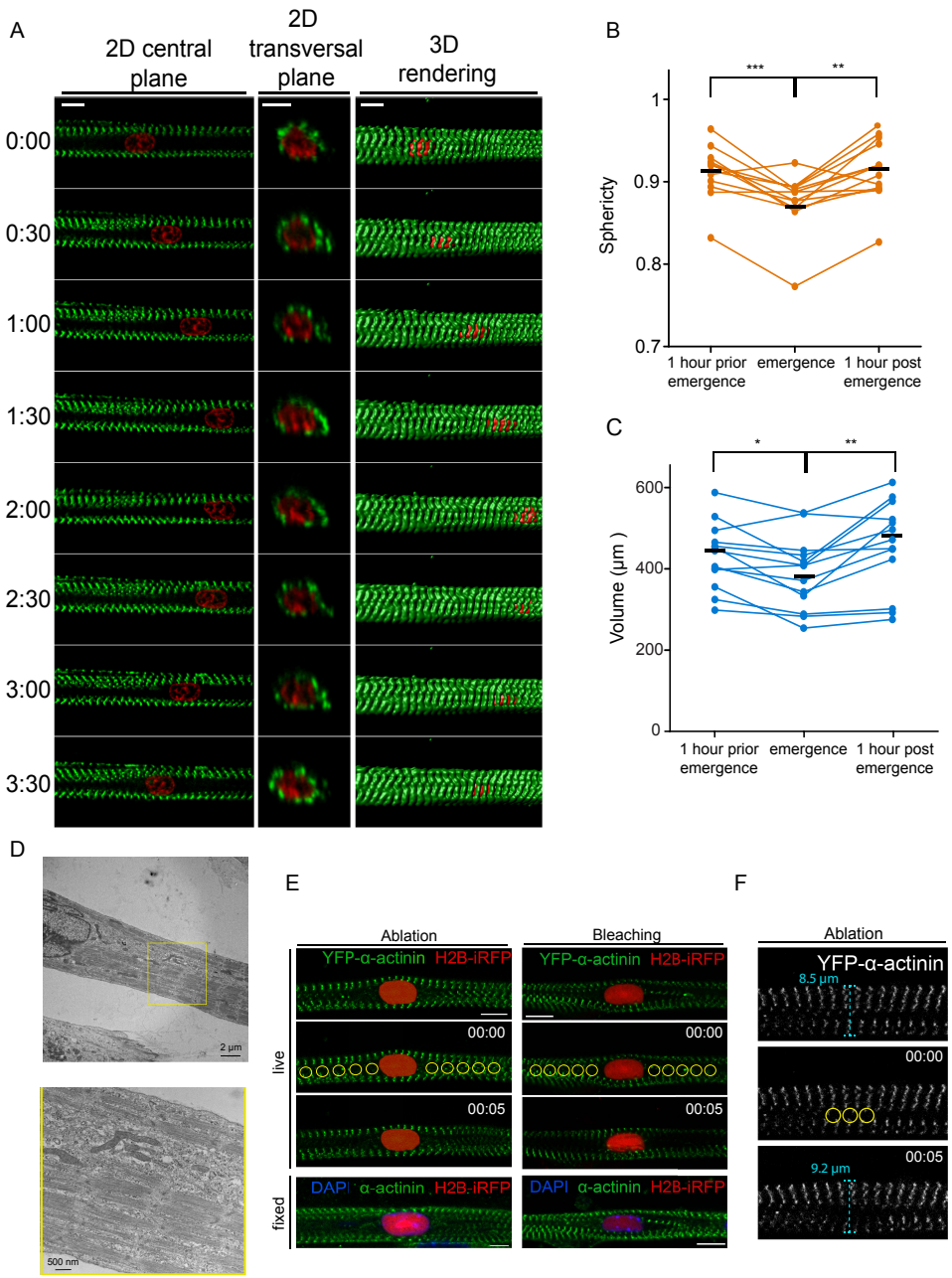

Supplementary Figure 1 Myofibril cross-linking induces forces on the nucleus. A. Kymograph from a time-lapse movie of a 4-day myofiber depicting a centrally located nucleus (H2B-iRFP, red) surrounded by myofibrils bundles (YFP-α-actinin, green) while moving longitudinally within these myofibrils Left: 2D view of the central plane. Middle: transversal view in the middle of the nucleus. Right: surface three-dimensional rendering. Time, hh:mm. Scale bar, 10 µm. B. Dot plot showing changes in sphericity 1 h before, at and after nuclear emergence of individual nuclei. Black lines represent the average. Data from 8 independent experiments were combined and error bars represent s.e.m from n = 8 nuclei. Wilcoxon matched-pairs signed ranked test was used to determine statistical significances, where *** $P < 0.001$, ** $P < 0.01$, NS, not significant. Source data is available in Supplementary Table 3. C. Dot plot showing changes in volume 1 h before, at and after nuclear emergence of individual nuclei. Black lines represent the average. Data from 8 independent experiments were combined and error bars represent s.e.m from n = 8 nuclei. Wilcoxon matched-pairs signed ranked test was used to determine statistical significances, where * $P < 0.05$. Source data is available in Supplementary Table 3. D. Longitudinal electron micrograph of a 4-5 day myofiber depicting area devoid of myofibrils. Scale bar, 2 µm. 4x Magnification corresponding to the yellow square is shown on the right of the image. Image shown is representative of 5 experiments. E. Representative image of a 4.5-day myofiber before (00:00) and after (00:05) laser ablation or bleaching with myofibrils depicted in green (YFP-α-actinin) and the nucleus in red (H2B-iRFP). Yellow circles represent ablated or bleached areas. Scale bar, 10 µm. 00:00 (hh:mm). Bottom panel represent correlative immunofluorescence microscopy of myofibers above, fixed right after 00:05 but stained for myofibrils (α-actinin, green) and nucleus (DAPI, blue). Scale bar, 10 µm. Image shown is representative of 6 experiments. F. Representative image of a 4.5-day myofiber before and after laser ablation and tagged for z-lines (YFP-α-actinin). Yellow circles represent ablated areas and blue dashed line represents thickness of myofiber. 00:00 (hh:mm). Image shown is representative of 6 experiments.

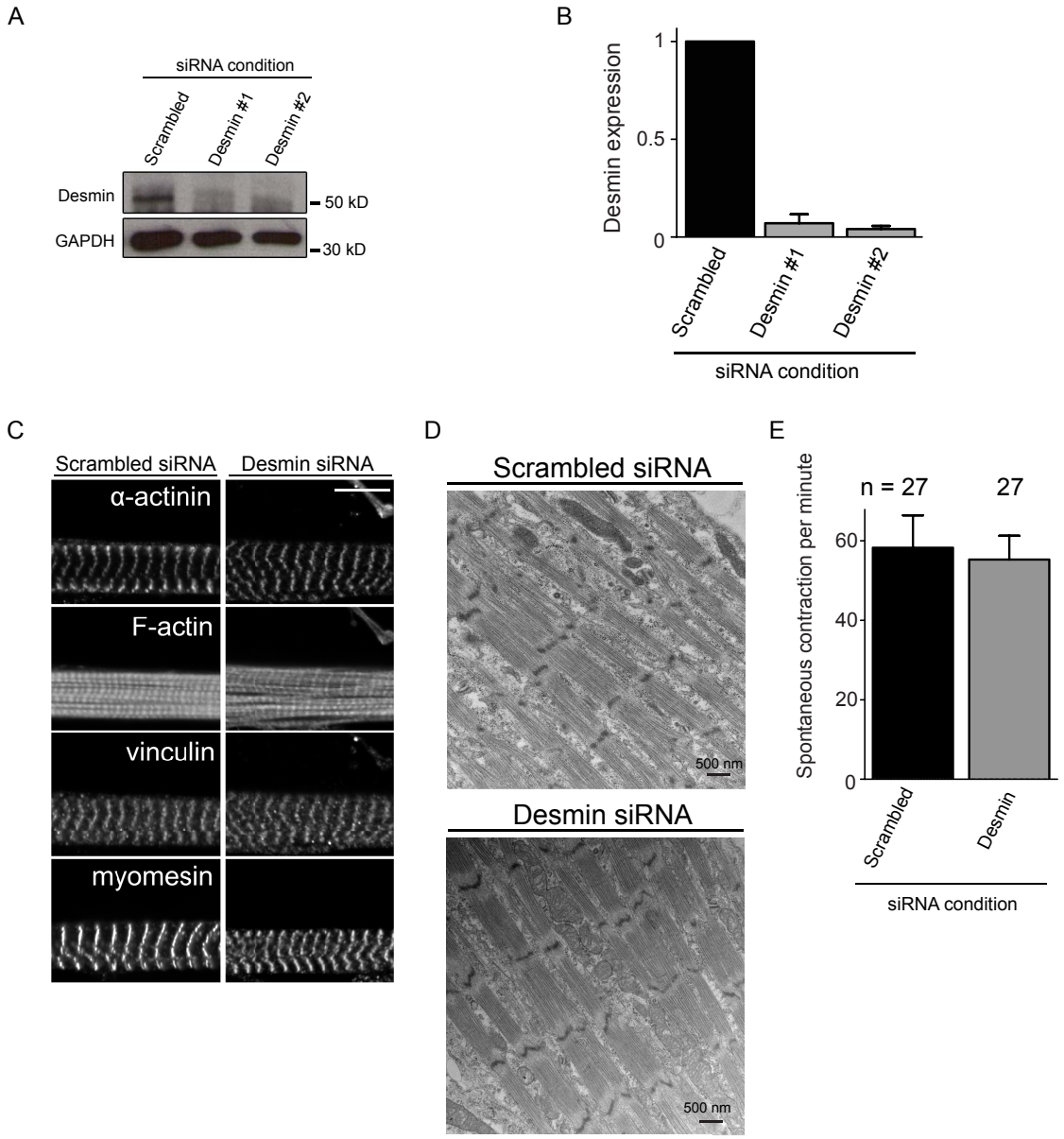

Supplementary Figure 2 Desmin knock down does not affect myofibril integrity. A. Western blot with indicated antibodies from 10-day myofibers knocked down for scrambled or desmin. Blots were repeated 3 times. B. Bar chart plotting desmin expression in 10-day myofibers knocked down for scramble or desmin. Error bars represent s.e.m from 3 independent experiments. C. Representative immunofluorescence image of 5-day myofibers knocked down for scrambled or desmin and stained for myofibril integrity markers: α-actinin, F-actin, vinculin and myomesin. Scale bar, 10 μm. Image shown is representative of 4 experiments. D. Representative electron micrograph of 5-day myofibers knocked down for scrambled or desmin showing myofibril integrity. Scale bar, 500 nm. Image shown is representative of 5 experiments. E. Bar chart plotting number of spontaneous contraction per minute in myofibers knocked-down for scrambled or desmin. Data from 3 independent experiments were combined and error bars represent s.e.m from indicated *n* myofibers for each cohort. Source data is available in Supplementary Table 3.

A

Actin name	Abbreviation	Gene symbol	Expression
Actin alpha 1, skeletal muscle	α-$_{sk}$-actin	Acta1	Skeletal muscle
Actin alpha 2, smooth muscle	α-$_{sm}$-actin	Acta2	Smooth muscle, aorta
Actin alpha, cardiac 1	α-$_{ca}$-actin	Actc1	Heart
Actin beta 1	β-actin	Actb1	Ubiquitous
Actin gamma 1	γ-actin	Actg1	Ubiquitous
Actin gamma 2, smooth muscle	γ-$_{sm}$-actin	Actg2	Smooth muscle

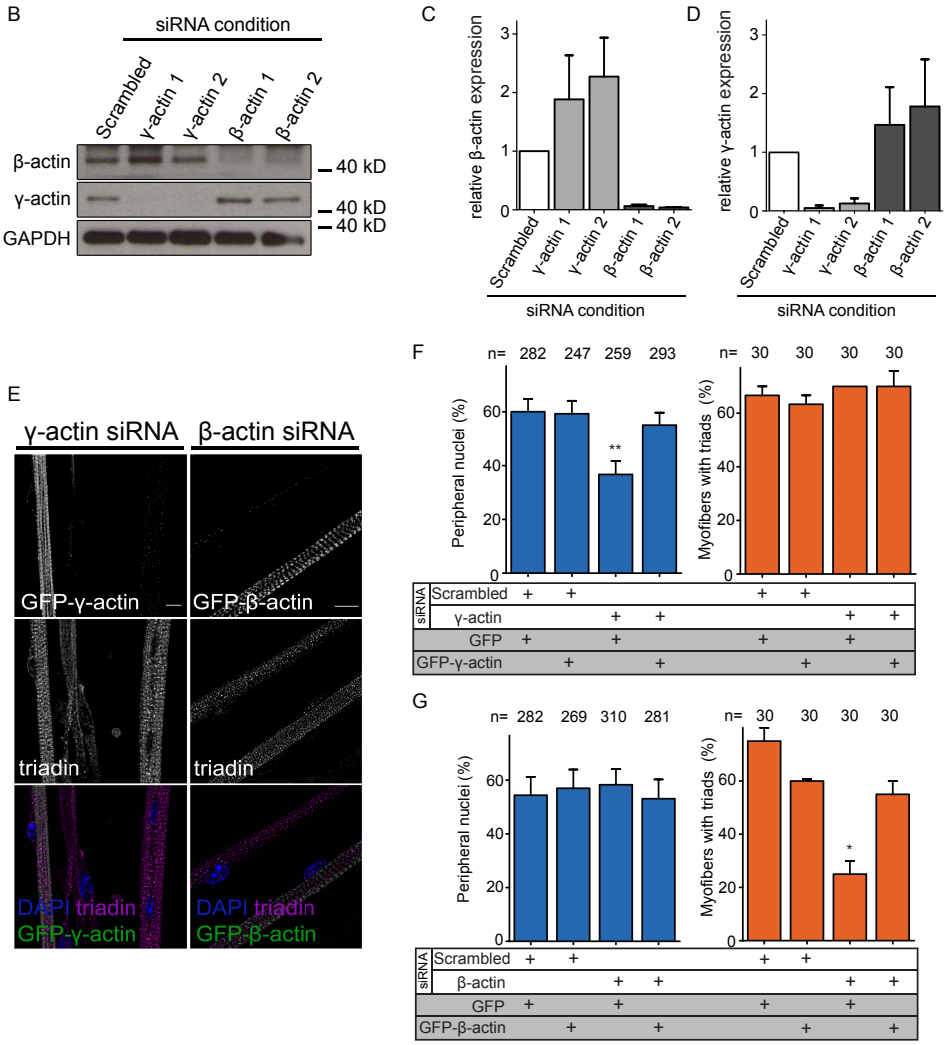

Supplementary Figure 3 β- and γ-actin knockdown down confirmation and rescue. A. Table enumerating different actin isoforms. B. Western blot with indicated antibodies from 10-day myofibers knocked down for scrambled, γ-actin or β-actin. Blots were repeated 3 times. C, Bar chart plotting β-actin expression in 10-day myofibers knocked down for scrambled, γ-actin or β-actin. Error bars represent s.e.m from 3 independent experiments. D. Bar chart plotting γ-actin expression in 10-day myofibers knocked down for scrambled, γ-actin or β-actin. Error bars represent s.e.m from 3 independent experiments. E. Representative immunofluorescence images of 10-day myofibers knocked down for γ-actin or β-actin and transfected with siRNA resistant GFP-γ-actin (green) and GFP-β-actin (green), respectively, and stained for triadin (triad marker, magenta) and DAPI (blue). Scale bar, 10 μm. Image shown is representative of 3 experiments. F. Quantification of peripheral nuclei positioning and traversal triads in 10-day myofibers expressing either GFP or the siRNA resistant GFP-γ-actin construct and knocked down either with scrambled or γ-actin. Data from 3 independent experiments were combined and error bars represent s.e.m from indicated *n* nuclei or myofibers for each cohort. Unpaired t-test was used to determine statistical significances, where *** P < 0.01*. Source data is available in Supplementary Table 3. G. Quantification of peripheral nuclei positioning and traversal triads in 10-day myofibers expressing either GFP or the siRNA resistant GFP-β-actin construct and knocked down either with scrambled or β-actin. Data from 3 independent experiments were combined and error bars represent s.e.m from indicated *n* nuclei or myofibers for each cohort. Unpaired t-test was used to determine statistical significances, where * P < 0.05*. Source data is available in Supplementary Table 3.

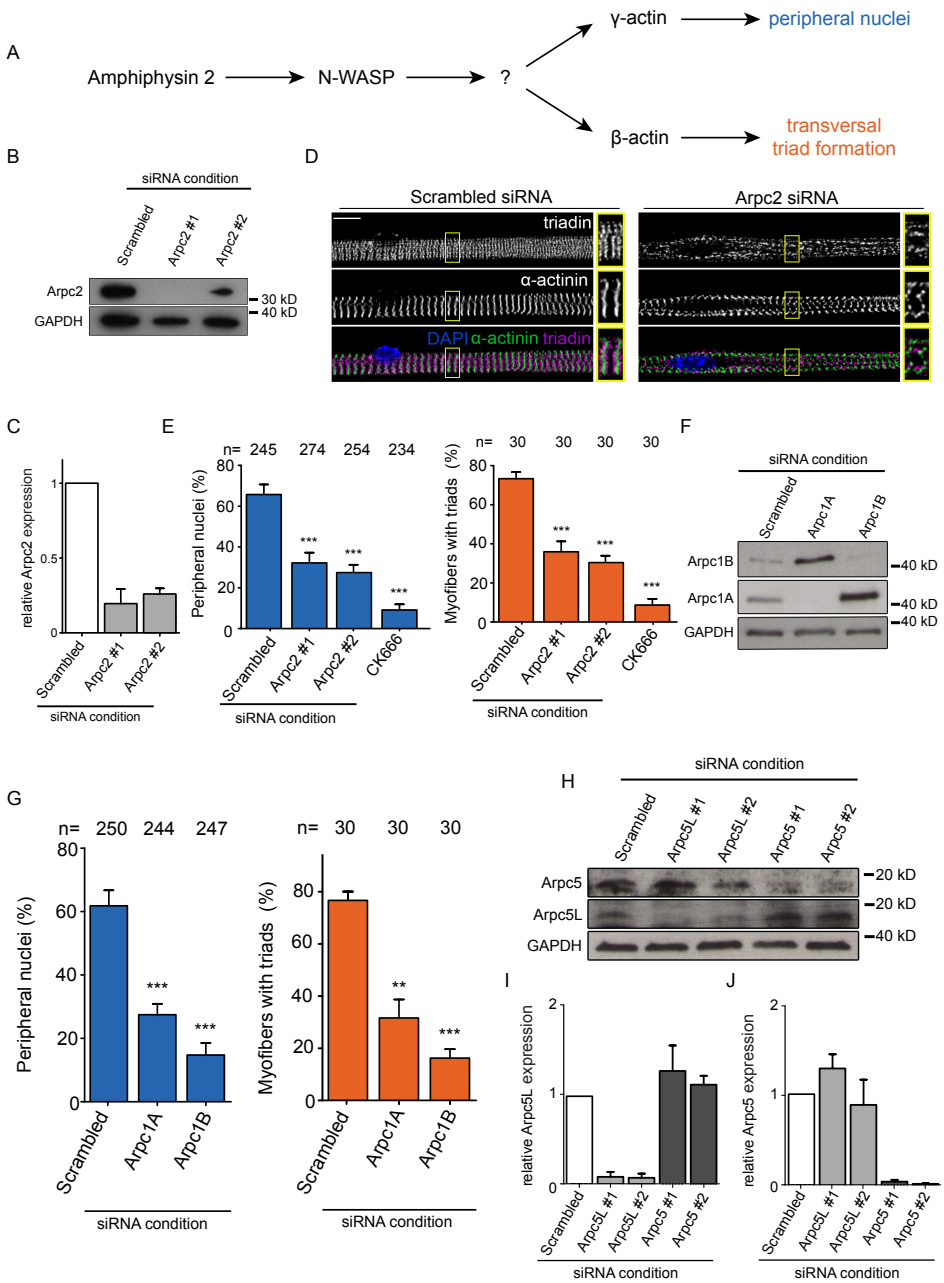

Supplementary Figure 4 Arp subunits knockdown confirmation and quantification. A. Schematic representation of the pathways that regulate peripheral nuclear position and transversal triad formation. B. Western blot with indicated antibodies from 10-day myofibers knocked down for scrambled or Arpc2. Blots were repeated 3 times. C. Bar chart plotting Arpc2 expression in 10-day myofibers knocked down for scrambled or Arpc2. Error bars represent s.e.m from 3 independent experiments. D. Representative immunofluorescence images of 10-day myofibers knocked down for scrambled or Arpc2 and stained with triadin (triad marker, magenta), α-actinin (myofibrils/Z-line marker, green) and DAPI (nucleus, blue). Scale bar, 10 µm. 2x Magnifications corresponding to the yellow squares are showed in the right of each image. Image shown is representative of 3 experiments. E. Quantification of peripheral nuclei positioning (left) and transversal triads (right) in 10-day myofibers knocked down for scrambled or Arpc2, or treated with the Arp2/3 inhibitor CK666. Data from 3 independent experiments were combined and error bars represent s.e.m from indicated *n* nuclei or myofibers for each cohort. Unpaired t-test was used to determine statistical significances, where **** P < 0.001*. Source data is available in Supplementary Table 3. F. Western blot with indicated antibodies from 10-day myofibers knocked down for scrambled, Arpc1A or Arpc1B. Blots were repeated 3 times. G. Quantification of peripheral nuclei (left) and transversal triads (right) in 10-day myofibers knocked down for scrambled, Arpc1A or Arpc1B. Data from 4 independent experiments were combined and error bars represent s.e.m from indicated *n* nuclei or myofibers for each cohort. Unpaired t-test was used to determine statistical significances, where **** P < 0.001*, *** P < 0.01*. Source data is available in Supplementary Table 3. H. Western blot with indicated antibodies from 10-day myofibers knocked down for scrambled, Arpc5L or Arpc5. Blots were repeated 3 times. I. Bar chart plotting Arpc5L expression in 10-day myofibers knocked down for scrambled, Arpc5L or Arpc5. Error bars represent s.e.m from 3 independent experiments. J. Bar chart plotting Arpc5 expression in 10-day myofibers knocked down for scrambled, Arpc5L or Arpc5. Error bars represent s.e.m from 3 independent experiments.

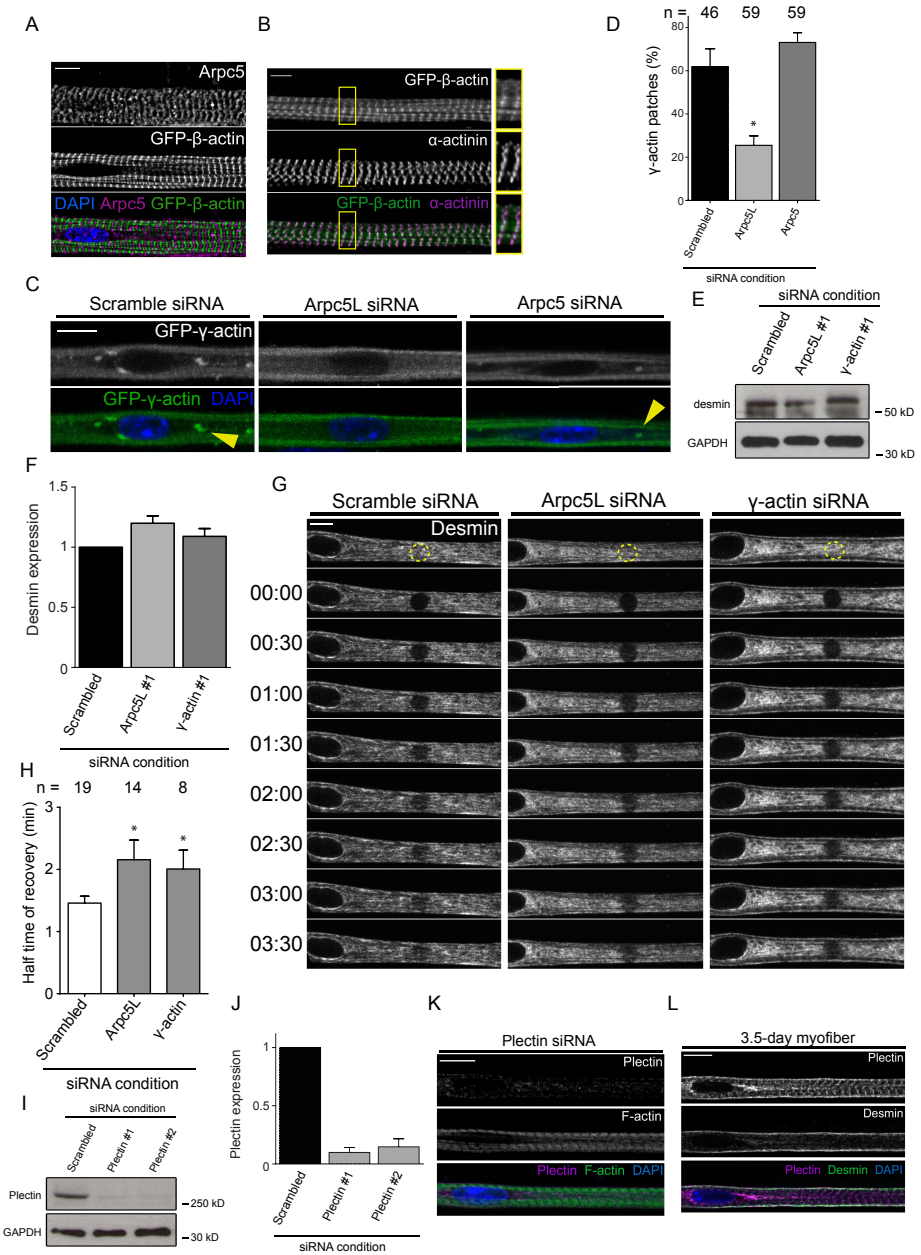

Supplementary Figure 5 Arpc5L and γ-actin involvement in desmin organization independent of plectin. A. Representative immunofluorescence images of 5-day myofibers expressing GFP-β-actin (green) and immunostained for Arpc5 (magenta). Scale bar, 10 µm. Image shown is representative of 7 experiments. B. Representative immunofluorescence image of a 5-day myofiber transfected with GFP-β-actin (green) and stained for α-actinin (myofibrils/Z-line marker, magenta). 2x Magnifications corresponding to the yellow squares are showed in the right of each image. Scale bar, 10 µm. Image shown is representative of 7 experiments. C. Representative immunofluorescence image of a 5-day myofiber transfected with GFP-γ-actin (green) and knocked down scrambled, Arpc5L or Arpc5. Yellow arrow heads represent γ-actin accumulation. Scale bar, 10 µm. Image shown is representative of 4 experiments. D. Bar chart plotting γ-actin accumulation in between myofibrils and next to nuclei in scrambled, Arpc5L or Arpc5 knocked down myofibers. Source data is available in Supplementary Table 3. E. Western blot with indicated antibodies from 10-day myofibers knocked down for scrambled, Arpc5L or γ-actin. Blots were repeated 3 times. F. Bar chart plotting desmin expression in 10-day myofibers knocked down for scrambled, Arpc5L or γ-actin. Error bars represent s.e.m from 3 independent experiments. G. Confocal fluorescence images from a representative FRAP experiment of EmGFP-desmin before transversal organization in 4.5-day myofibers knocked down for scramble, Arpc5L or γ-actin. The dashed yellow circles show bleached regions. Time 00:00 (min:sec). Scale bar, 10 µm. H. Average half-time of recovery of EmGFP-desmin in 4.5-day myofibers knocked down for scramble, Arpc5L or γ-actin following photobleaching. Data from 3 independent experiments were combined and error bars represent s.e.m from indicated *n* myofibers for each cohort. Unpaired t-test was used to determine statistical significances, where $* P < 0.05$. Source data is available in Supplementary Table 3. I. Western blot with indicated antibodies from 10-day myofibers knocked down for scrambled or plectin. Blots were repeated 3 times. J. Bar chart plotting desmin expression in 10-day myofibers knocked down for scramble or plectin. Error bars represent s.e.m from 3 independent experiments. K. Representative immunofluorescence image of a 4.5-day myofiber knocked down for plectin and stained for F-actin (phalloidin, green), plectin (magenta) and DAPI (nucleus, blue). Scale bar, 10 µm. Image shown is representative of 3 experiments. L. Representative immunofluorescence image of a 3.5-day myofiber stained for plectin (magenta), desmin (green) and DAPI (nucleus, blue). Scale bar, 10 µm. Image shown is representative of 3 experiments.

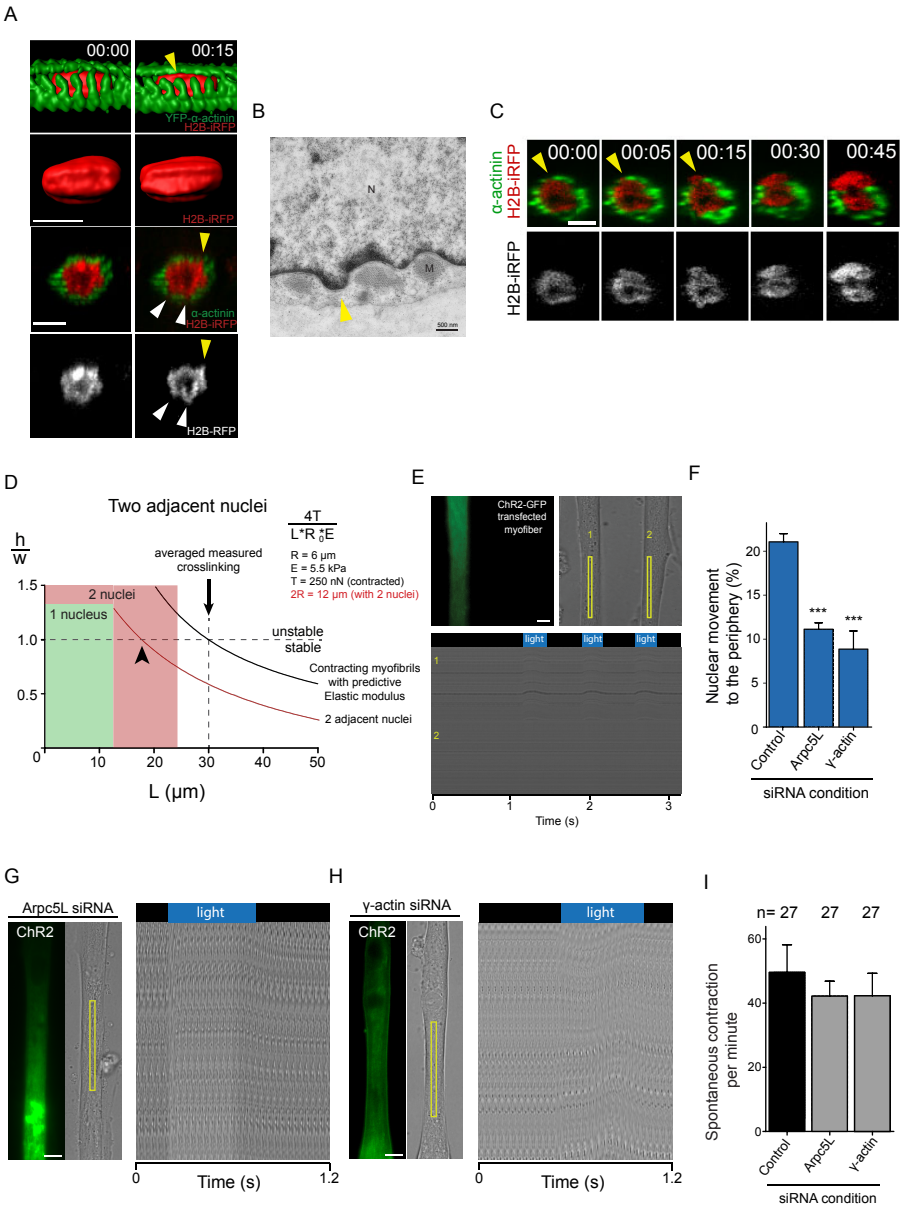

Supplementary Figure 6 Nuclear wrinkles A. Nucleus (H2B-iRFP, red) and myofibrils (YFP-α-actinin, green) from a 4.5-day myofiber in a 15 minute interval without (left, 00:00) and with (right, 00:15) pronounced wrinkles. Top 2 frames: longitudinal surface three-dimensional rendering of the nucleus (red) and myofibrils (green). Bottom 2 frames: orthogonal view of the nucleus (red) and myofibrils (green). Yellow arrowhead represents the same wrinkle and white arrowheads represent other wrinkles. Scale bar, 10 μm. B. Representative transversal electron micrograph of 4-day myofibers knocked depicting a nuclear wrinkle. Scale bar, 500 nm. Image shown is representative of 5 experiments. C. Orthogonal view of a nucleus (red) and myofibrils (green) during nuclear movement to the periphery evolving from a wrinkle to a protrusion (yellow arrow head). Time, hh:mm. Scale bar, 10 μm. D. Model prediction of the stability of wrinkles relative to force on the nucleus when two nuclei are adjacent. The scaled wrinkle size h/w is plotted as a function of crosslinking L based on the function $4T/L*R_0*E$. Above the threshold $h/w \approx 1$, the wrinkle becomes an unstable bud and the nucleus is moved to the periphery. Black line represents optimal values to reach the instability threshold. Red line represents values for two adjacent nuclei. Green and red boxes represent minimal space occupied by one or two nuclei respectively where crosslinking is not possible. E. Top: Representative epi-fluorescent (left) and bright-field light image (right) of the first frame from time-lapse movie of two 3.5-day myofibers, one transfected with the ChR2-GFP and the other untransfected. Bottom: Kymograph of the region in yellow from the top right panel and showing contraction when blue light is emitted (blue boxes). Scale bar, 10 μm. F. Quantification of nuclei migrating to the periphery from a 24-hour time-lapse movie in 3.5-day untransfected myofibers (control) and myofibers expressing ChR2-GFP alone (ChR2) or knocked down for either Arpc5L or γ-actin. Data from 4 independent experiments were combined and error bars represent s.e.m from indicated *n* nuclei for each cohort. Unpaired t-test was used to determine statistical significances, where **** P < 0.001*. Source data is available in Supplementary Table 3. G. left: Representative epi-fluorescent and bright-field light image of the first frame from time-lapse movie of a 3.5-day myofibers transfected with ChR2-GFP and knocked down for Arpc5L. right: Kymograph of the region in yellow from the left panel and showing contraction when blue light is emitted (blue boxes). Scale bar, 10 μm. H. left: Representative epi-fluorescent and bright-field light image of the first frame from time-lapse movie of a 3.5-day myofibers transfected with ChR2-GFP and knocked down for γ-actin. right: Kymograph of the region in yellow from the left panel and showing contraction when blue light is emitted (blue boxes). Scale bar, 10 μm.I. Bar chart plotting number of spontaneous contraction per minute in myofibers knocked-down for Arpc5L and γ-actin. Data from 3 independent experiments were combined and error bars represent s.e.m from indicated *n* myofibers for each cohort.

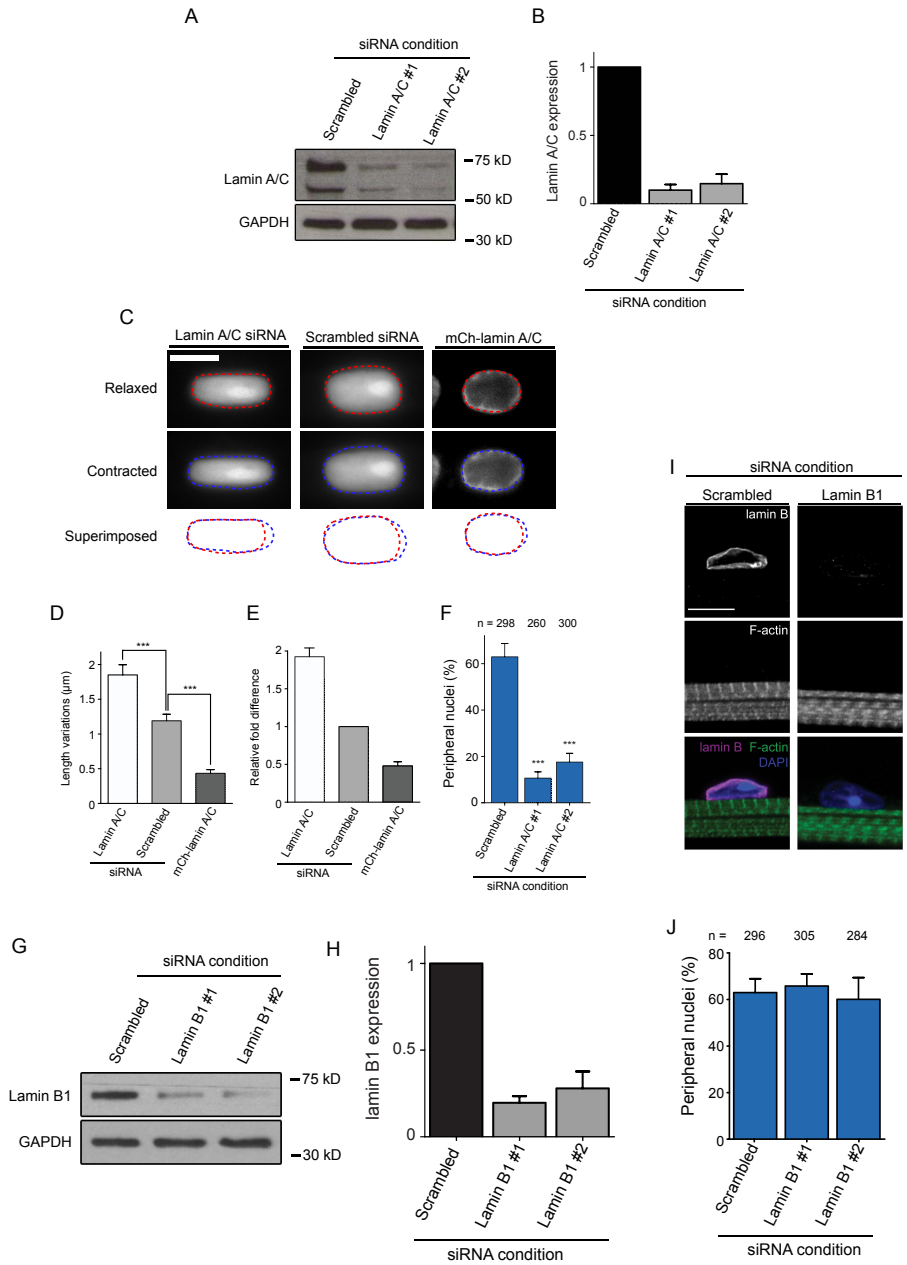

Supplementary Figure 7 Lamin knockdown confirmation and quantification. A. Western blot with indicated antibodies from 10-day myofibers knocked down for scrambled or lamin A/C. Blots were repeated 3 times. B. Bar chart plotting lamin A/C expression in 10-daymyofibers knocked down for scrambled or lamin A/C. Error bars represent s.e.m from 3 independent experiments. C. Representative immunofluorescence of nuclei before (relaxed) and during (contracted) myofiber contraction aligned . Myofibers were optogenetically induced to contract and transfected with either NLS-mCherry or mCh-lamin A/C and knocked down for scrambled or lamin A/C. Shape of the nucleus in a relaxed (dashed red) and contracted (dashed blue) myofiber were superimposed and aligned to the left to show length change on the right. Scale bar, 10 µm. Image shown is representative of 3 experiments. D. Bar chart plotting nuclear length variations before and during contraction in myofibers knocked down for scrambled, lamin A/C knocked down and mCh-lamin A/C. Data from 4 independent experiments were combined and error bars represent s.e.m from indicated ($n = 30$ nuclei) for each cohort. Unpaired t-test was used to determine statistical significances, where *** $P < 0.001$. Source data is available in Supplementary Table 3. E. Bar chart plotting relative fold increase (compared to scramble) of nuclear length before and during contraction in myofibers knocked down for scrambled, lamin A/C knocked down and mCh-lamin A/C. Absolute length differences were normalized on myofiber size to compensate for contraction force and then normalized on scramble. Source data is available in Supplementary Table 3. F. Quantification of peripheral nuclei positioning in 10-day myofibers knocked down for scrambled or lamin A/C. Data from 3 independent experiments were combined and error bars represent s.e.m from indicated *n* nuclei for each cohort. Unpaired t-test was used to determine statistical significances, where *** $P < 0.001$. Source data is available in Supplementary Table 3. G. Western blot with indicated antibodies from 10-day myofibers knocked down for scrambled or lamin B1. Blots were repeated 3 times. H. Bar chart plotting lamin B1 expression in 10-daymyofibers knocked down for scrambled or lamin B1. Error bars represent s.e.m from 3 independent experiments. I. Representative immunofluorescence image of a 10-day myofiber knocked down for scrambled or lamin B1 and stained for F-actin (phalloidin, green), lamin B1 (magenta) and DAPI (nucleus, blue). Scale bar, 10 µm. Image shown is representative of 3 experiments. J. Quantification of peripheral nuclei positioning in 10-day myofibers knocked down for scrambled or lamin B1. Data from 3 independent experiments were combined and error bars represent s.e.m from indicated *n* nuclei for each cohort. Unpaired t-test was used to determine statistical significances, where *** $P < 0.001$. Source data is available in Supplementary Table 3.

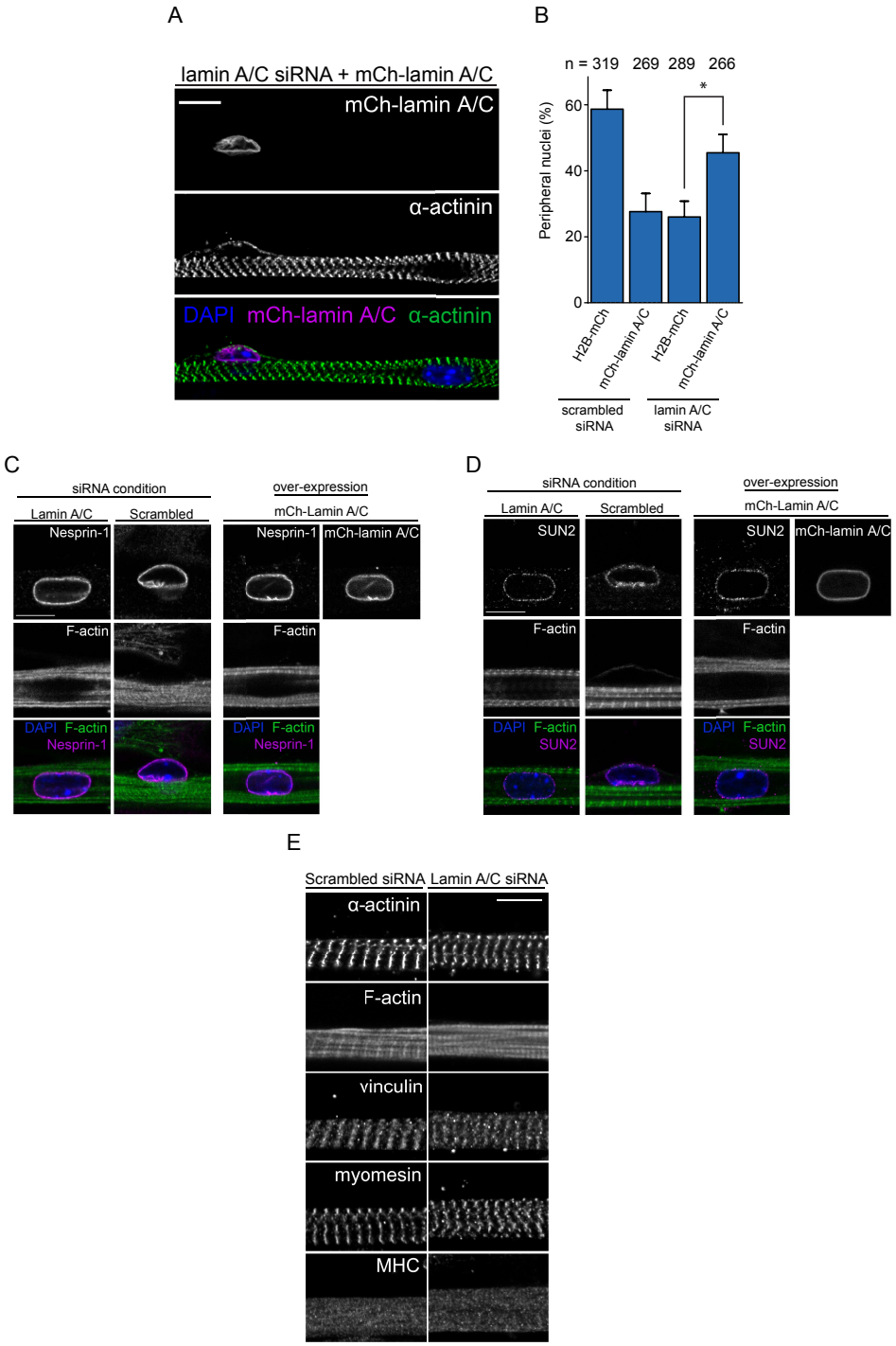

Supplementary Figure 8 Myofibril integrity in lamin knock down and nuclear rupture. A. Representative immunofluorescence image of 10-day myofibers knocked down for lamin A/C and rescued with an mCh-Lamin A/C construct (magenta) and stained for z-lines (α-actinin, green) and nucleus (DAPI, blue). Scale bar, 10 μm. Image shown is representative of 4 experiments. B. Quantification of peripheral nuclei positioning and traversal triads in 10-day myofibers knocked down for scrambled or desmin and transfected with either H2B-RFP or mCh-lamin A/C. Data from 4 independent experiments were combined and error bars represent s.e.m from indicated *n* nuclei or myofibers for each cohort. Unpaired t-test was used to determine statistical significances, where $* P < 0.05$. Source data is available in Supplementary Table 3. C. Representative immunofluorescence image of 5-day myofibers knocked down for scrambled or lamin A/C, or overexpressing mCh-lamin A/C and stained for Nesprin-1 (magenta), myofibrils (F-actin, green) and nucleus (DAPI, blue). Scale bar, 10 μm. Image shown is representative of 3 experiments. D. Representative immunofluorescence image of 5-day myofibers knocked down for scrambled or lamin A/C or overexpressing mCh-lamin A/C and stained for SUN2 (magenta), myofibrils (F-actin, green) and nucleus (DAPI, blue). Scale bar, 10 μm. Image shown is representative of 3 experiments. E. Representative immunofluorescence image of 10-day myofibers knocked down for scrambled or lamin A/C and stained for myofibril integrity markers: α-actinin, F-actin, vinculin and myomesin. Scale bar, 10 μm. Image shown is representative of 3 experiments.

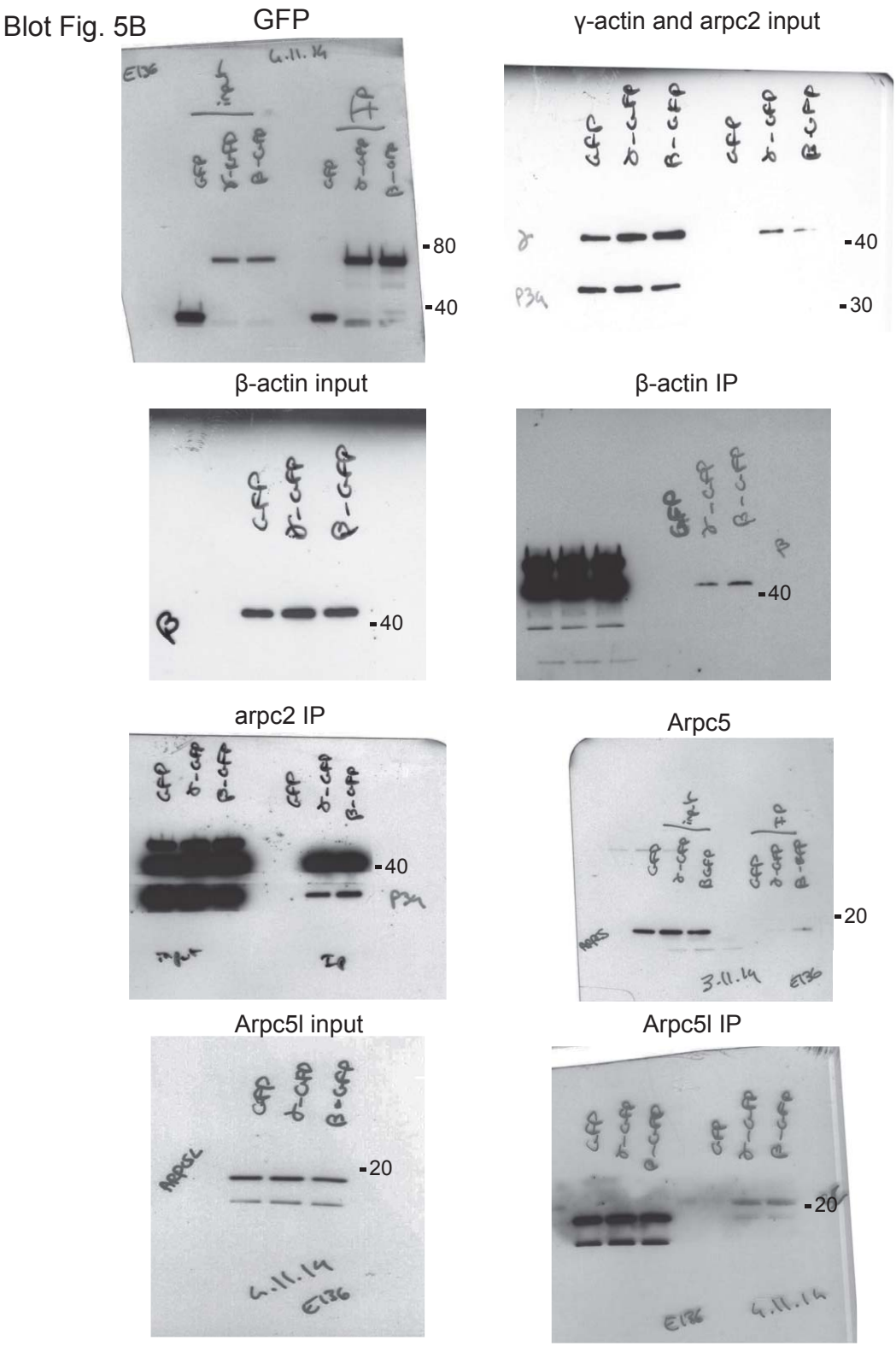

Supplementary Figure 9 Unprocessed scans of blots.

blot: Fig. 5A

GFP

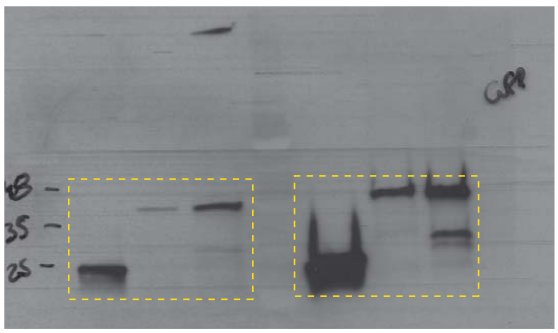

γ-actin input

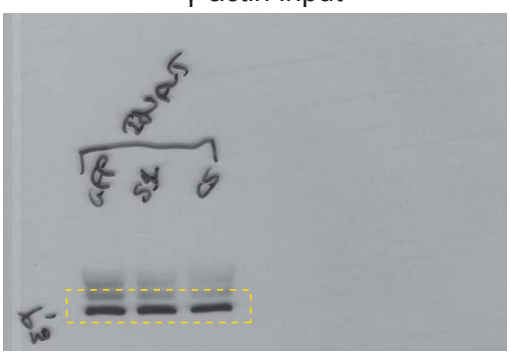

γ-actin IP

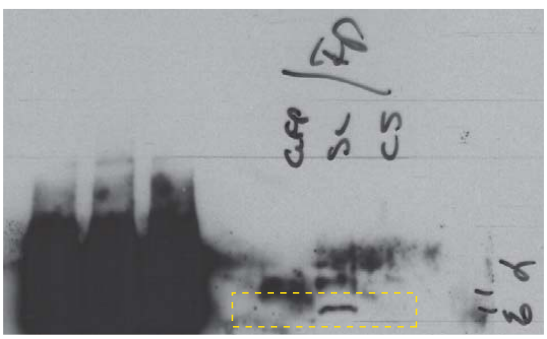

β-actin input

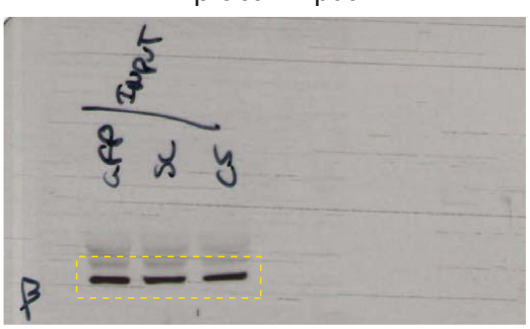

β-actin IP

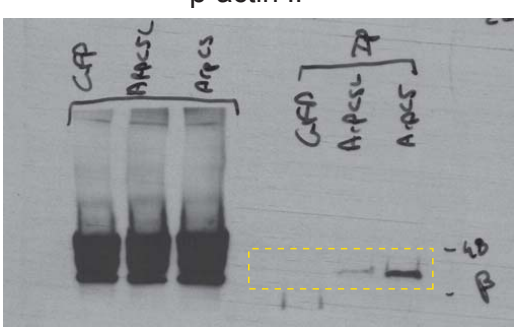

arpc2

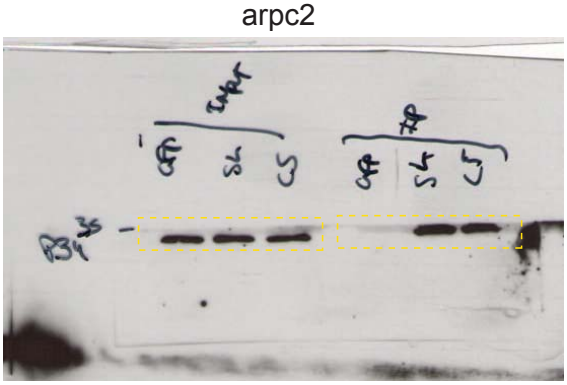

Supplementary Figure 9 Continued

Blot Fig. 5C

Arpc5

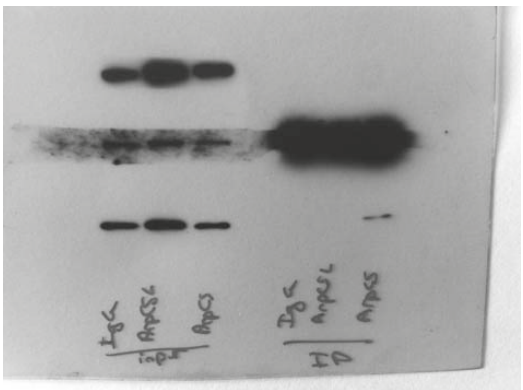

gamma actin

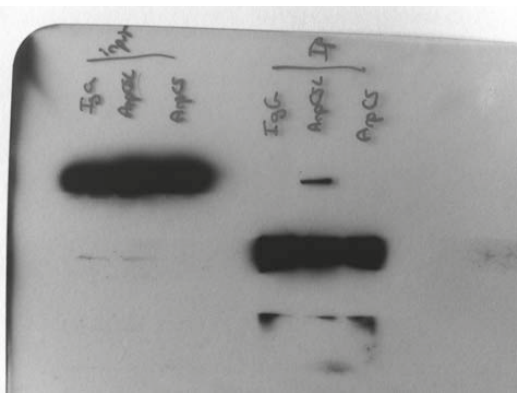

Arpc5L

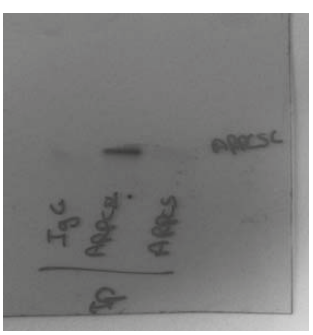

gamma actin

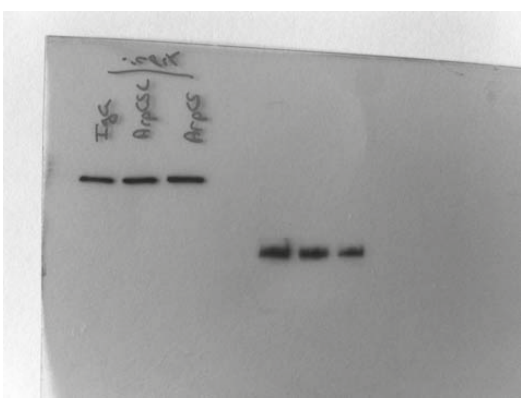

Blot Fig. S2A

Desmin and GAPDH

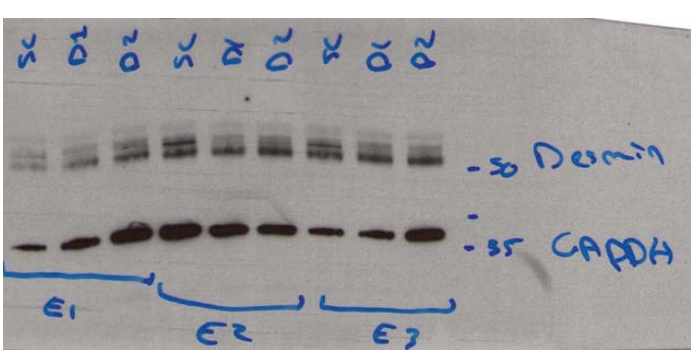

Supplementary Figure 9 Continued

Blot Fig. S3B

gamma actin

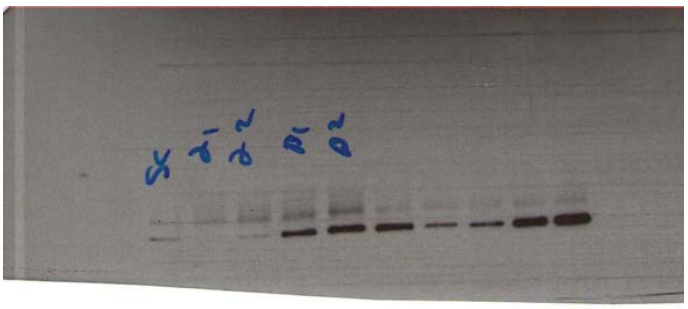

GAPDH

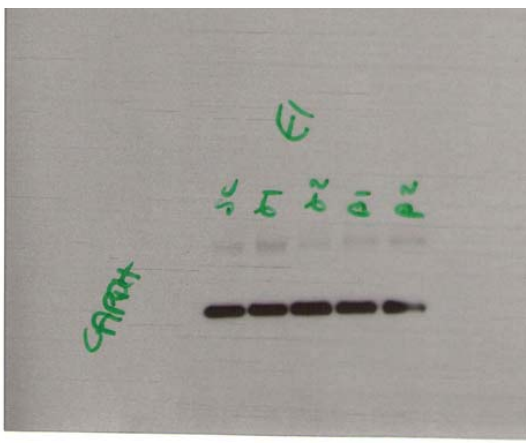

gamma actin

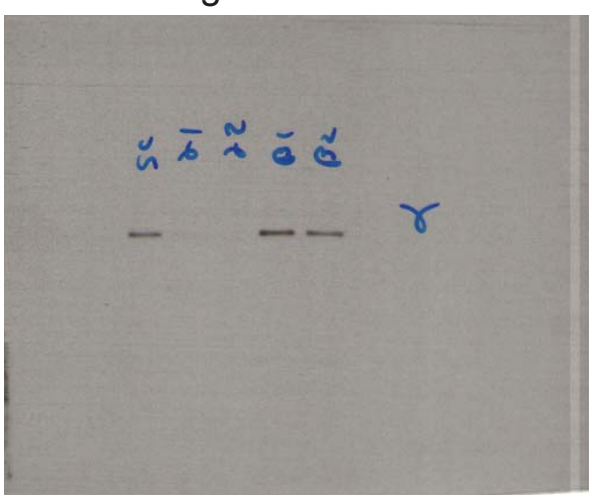

Blot Fig. S4H

Arpc5

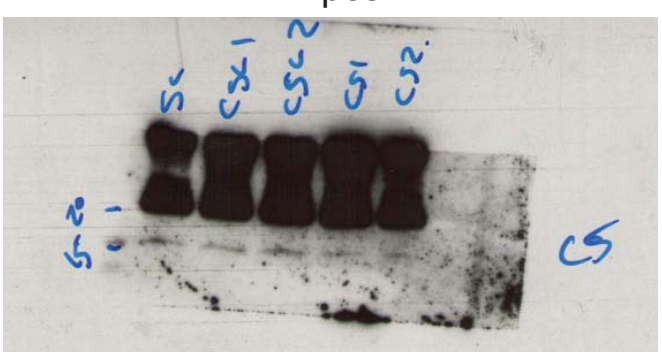

GAPDH

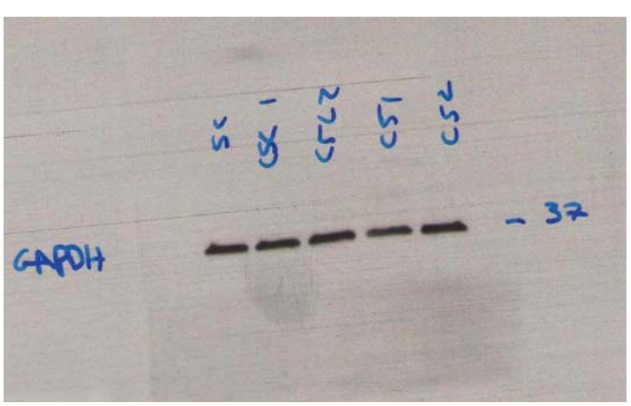

Arpc5L

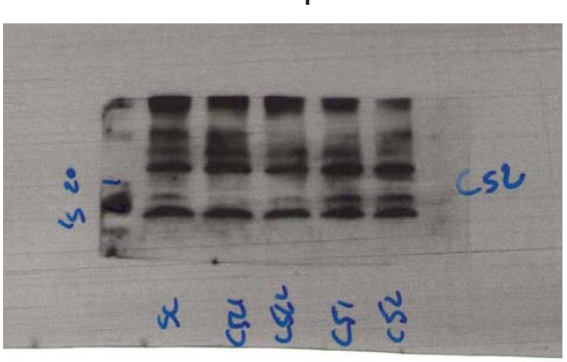

Supplementary Figure 9 Continued

Blot Fig. S5E

GAPDH

Desmin

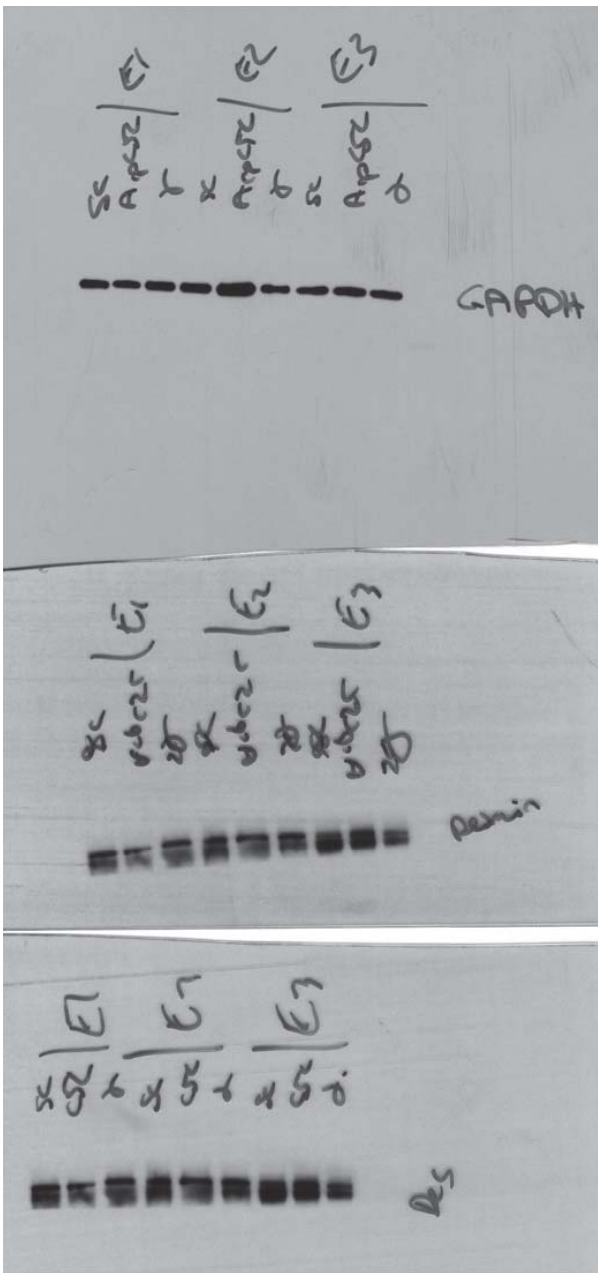

Blot Fig. S5I

GAPDH

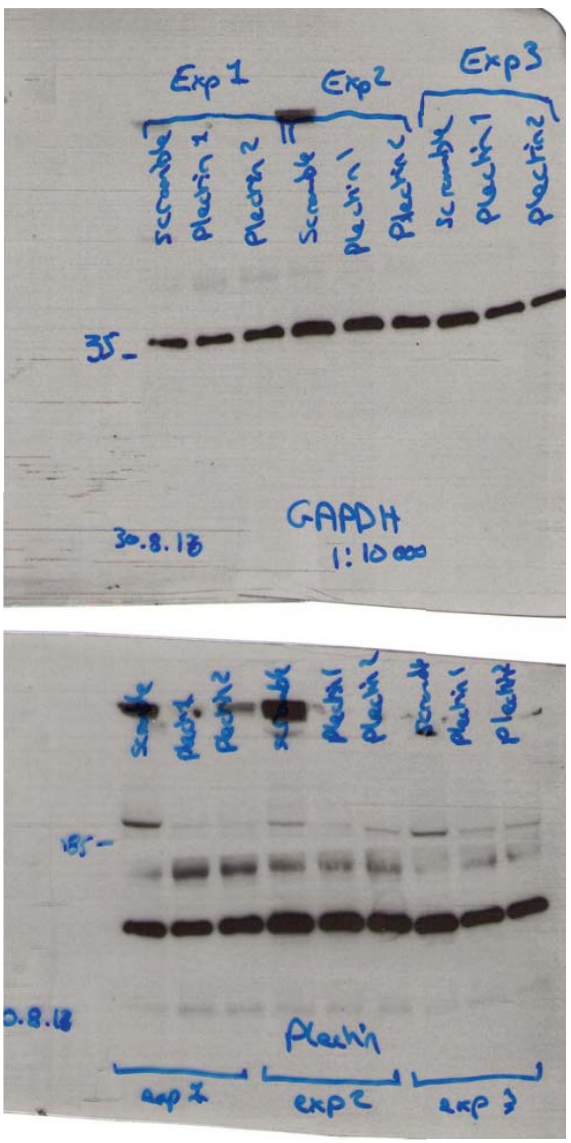

Plectin

Supplementary Figure 9 Continued

Blot Fig. S7A

Lamin A/C

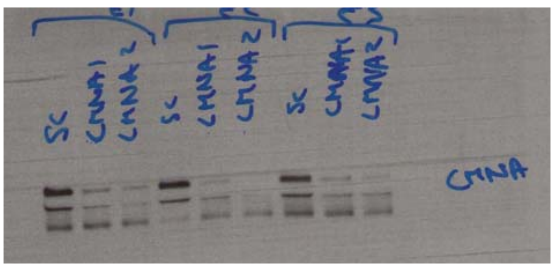

GAPDH

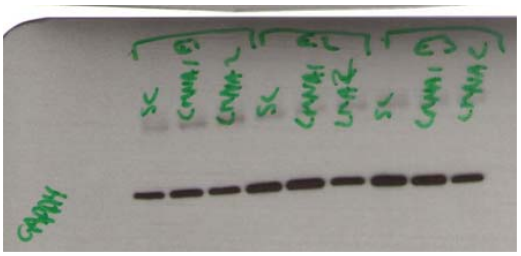

Blot Fig. S7G

Lamin B

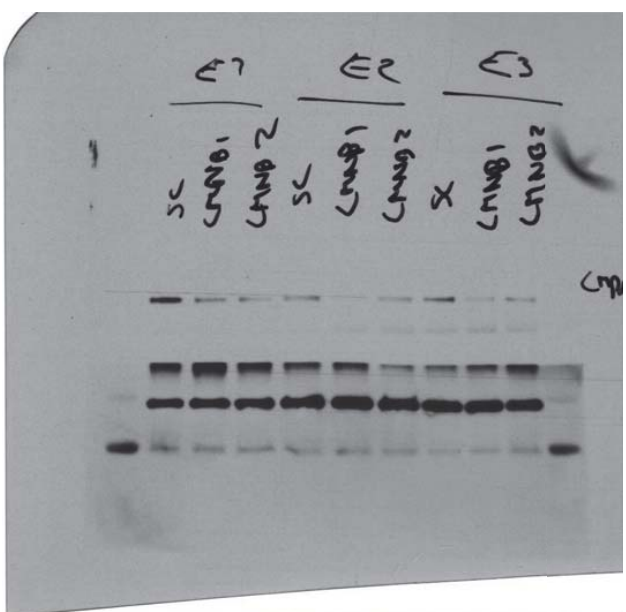

GAPDH

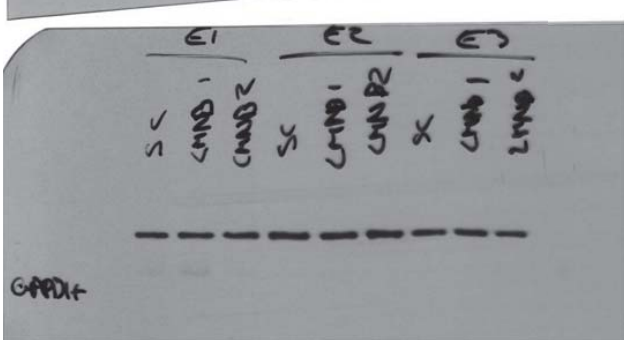

Supplementary Figure 9 Continued

Supplementary Table Legends

Supplementary Table 1 List of antibodies used in the study.

Supplementary Table 2 List of siRNA (with sequences) used in this study.

Supplementary Table 3 Source data collected for this study for figure panels Fig. 2A-B, 2D, 2F-G, 3B, 3E, 4C, 4G, 5F, 6I, 7A, 7C, 7D and 7H as well as supplementary figure panels S1B-C, S2E, S3F-G, S4E, S4G, S5D, S5H, S6F, S7D-E, S7F, S7J, S8B.

Supplementary Video Legends

Supplementary Video 1 Centrally located nucleus surrounded by myofibrils. Surface three-dimensional rendering of a time-lapse movie (also presented in Fig S3C) depicting a centrally located nucleus surrounded by myofibrils bundles while moving longitudinally in a 4-day myofiber expressing YFP-α-actinin (green, myofibrils) and H2B-iRFP (red, nucleus).

Supplementary Video 2 Nuclear movement to the periphery. Time-lapse movie of a 5-day myofiber depicting peripheral movement of a nucleus (red, H2B-iRFP) through myofibrils (green, α-YFP-actinin) (also presented in Fig 3A). Top left: top view of surface three-dimensional rendering. Middle left: side view of surface three-dimensional rendering. Bottom left: 2D view from the top of the central plane. Top right: nucleus alone viewed from 90° rotation surface three-dimensional rendering. Bottom right: nucleus with transparent myofibers from 90° rotation surface three-dimensional rendering

Supplementary Video 3 Nuclear wrinkles. Surface three-dimensional rendering of the same nucleus (red, H2B-iRFP) with more (wrinkled - right) or less (unwrinkled - left) wrinkles due to variations in myofibril tension rotating 360° along its longitudinal axis (also presented in Fig S5A).

Supplementary Video 4 Optogenetically controlled myofiber contraction. Time-lapse movie of 3.5-day myofibers transfected with ChR2-GFP (left) and untransfected (right) (also presented in Fig S5B). Blue light is shone at the rhythm of the "eye of the tiger" by Survivors to show controllability of contraction by light. We advise appropriate volume during video playback.

Supplementary Video 5 Nuclear movement to the periphery induced by myofiber contraction. Time-lapse movie of a 3.5-day myofiber transfected with ChR2-GFP (green) and H2B-iRFP (red) and untransfected (also presented in Fig 4F). Top: ChR2-GFP (green) and H2B-iRFP (red) channels. Bottom: H2B-iRFP (red) and bright-field (grey) channels. Blue light is shone 6 pulses per hour to induce contraction. 00:00 refers to 3.5 days.

nature research

Corresponding author(s): Edgar R. Gomes

☐ Initial submission ☐ Revised version ☒ Final submission

Life Sciences Reporting Summary

Nature Research wishes to improve the reproducibility of the work that we publish. This form is intended for publication with all accepted life science papers and provides structure for consistency and transparency in reporting. Every life science submission will use this form; some list items might not apply to an individual manuscript, but all fields must be completed for clarity.

For further information on the points included in this form, see Reporting Life Sciences Research. For further information on Nature Research policies, including our data availability policy, see Authors & Referees and the Editorial Policy Checklist.

Experimental design

1. Sample size

Describe how sample size was determined.

All experiments were performed at least 3 times independently and sample size was sufficient for most experiments. However, for statistics with an n lower than 10, a statistical power test was performed using GPower 3.1 to determine sample size appropriateness.

2. Data exclusions

Describe any data exclusions.

Outliers were detected using Gribbs' test at a P value < 0.05.

3. Replication

Describe whether the experimental findings were reliably reproduced.

Experiments were all reproducible.

4. Randomization

Describe how samples/organisms/participants were allocated into experimental groups.

Cell culture dishes obtained were randomly distributed into experimental groups.

5. Blinding

Describe whether the investigators were blinded to group allocation during data collection and/or analysis.

Investigators were blinded for most quantifications with one scientist generating the cells and another quantifying.

Note: all studies involving animals and/or human research participants must disclose whether blinding and randomization were used.

6. Statistical parameters

For all figures and tables that use statistical methods, confirm that the following items are present in relevant figure legends (or in the Methods section if additional space is needed).

n/a	Confirmed
☐	☒ The exact sample size (*n*) for each experimental group/condition, given as a discrete number and unit of measurement (animals, litters, cultures, etc.)
☐	☒ A description of how samples were collected, noting whether measurements were taken from distinct samples or whether the same sample was measured repeatedly
☐	☒ A statement indicating how many times each experiment was replicated
☐	☒ The statistical test(s) used and whether they are one- or two-sided (note: only common tests should be described solely by name; more complex techniques should be described in the Methods section)
☒	☐ A description of any assumptions or corrections, such as an adjustment for multiple comparisons
☐	☒ The test results (e.g. *P* values) given as exact values whenever possible and with confidence intervals noted
☐	☒ A clear description of statistics including central tendency (e.g. median, mean) and variation (e.g. standard deviation, interquartile range)
☐	☒ Clearly defined error bars

See the web collection on statistics for biologists for further resources and guidance.

Software

Policy information about availability of computer code

7. Software

Describe the software used to analyze the data in this study.	Graphpad was used to analyze statistics and Imaris was used to assess nuclear volume and sphericity. Algorithms for Imaris can be found here: http://www.bitplane.com/resources.aspx

For manuscripts utilizing custom algorithms or software that are central to the paper but not yet described in the published literature, software must be made available to editors and reviewers upon request. We strongly encourage code deposition in a community repository (e.g. GitHub). *Nature Methods* guidance for providing algorithms and software for publication provides further information on this topic.

Materials and reagents

Policy information about availability of materials

8. Materials availability

Indicate whether there are restrictions on availability of unique materials or if these materials are only available for distribution by a for-profit company.	All materials are available.

9. Antibodies

Describe the antibodies used and how they were validated for use in the system under study (i.e. assay and species).	Antibodies were mostly commercially available. Gamma and beta-actin were obtained from from Christelle Chaponnier's lab which were confirmed in a previous publication (doi: 10.12688/f1000research.8154.2). All antibody information is in Supplementary Table 1.

10. Eukaryotic cell lines

a. State the source of each eukaryotic cell line used.	no eukaryotic cell lines were used
b. Describe the method of cell line authentication used.	no eukaryotic cell lines were used
c. Report whether the cell lines were tested for mycoplasma contamination.	no eukaryotic cell lines were used
d. If any of the cell lines used are listed in the database of commonly misidentified cell lines maintained by ICLAC, provide a scientific rationale for their use.	no eukaryotic cell lines were used

Animals and human research participants

Policy information about studies involving animals; when reporting animal research, follow the ARRIVE guidelines

11. Description of research animals

Provide details on animals and/or animal-derived materials used in the study.	Primary myoblasts were isolated from 5 - 7 day old pups of C57BL/6 mice. Cells were grouped irregardless of gender. In vivo clearing and myofiber isolation was performed on newborn mice.

Policy information about studies involving human research participants

12. Description of human research participants

Describe the covariate-relevant population characteristics of the human research participants.	No human material was used for this study.